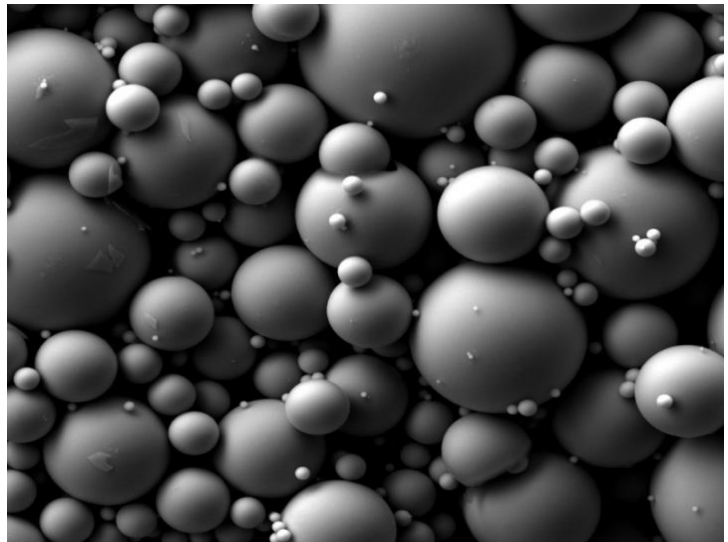




FunGlass School 2019/part 1

Book of Abstracts



Čertov, May 20-22, 2019

ORGANIZING INSTITUTIONS:



FunGlass School 2019 / Part 1

Book of Abstracts

Čertov, May 20-22, 2019

SCIENTIFIC BOARD: Dušan Galusek, Prof., DSc., Marek Liška, Prof., DSc.

REVIEWERS: Dušan Galusek, Prof., DSc., Marek Liška, Prof. DSc., Mária Chromčíková, Assoc.Prof., Robert Klement, Assoc.Prof., Alfonz Pliško, Assoc. Prof., Dr. Nasima Afsharimani, Dr. Martin Michálek, Dr. Jozef Kraxner, Dr. Nasima Afsharimani

Edited by Fatih Kurtuldu, Fulden Doğrul, Nurşen Mutlu, Susanta Sengupta and Vanda Mokráňová

ISBN 978-80-8075-874-5
EAN 9788080758745

This conference is part of a project that has received funding from the **European Union's Horizon 2020 research and innovation programme under grant agreement N°739566**



FunGlass
centre for functional and
surface functionalized glass

Table of Contents

A. Dasan / Development of 3D Bioactive Silicate Based Glass-Ceramic Scaffolds with Hierarchical Porosity by Additive Manufacturing.....	1
Z. Neščáková / Sol-gel derived Zn-doped mesoporous bioactive glasses for biomedical applications	3
Z. Vargas / Magnetic Mesoporous Silica Nanocomposites based on SBA-15/Fe₃O₄ as Multifunctional Nanoplatfroms for Technological Applications.....	4
F. Dogrul / Production of SiOC Based Bioactive Glass for Bone-Tissue Applications.....	6
F. Kurtuldu / Synthesis of Cerium and Gallium Doped Mesoporous Bioactive Glass Nanoparticles	8
N. Mutlu / Incorporation of Zinc Doped Borate Bioactive Glasses into Soft Matrices for Wound Healing Applications.....	10
S. Sengupta / Magnetic Bioactive Materials for Bone Regeneration and Tissue Engineering.....	12
N. Afsharimani / Sol-gel based hybrid coatings for corrosion protection of AA2024-T3 alloys.....	14
M. Žitňan / Inkjet printing of ceramic precursors based on sol-gel media	16
I. Petříková / Passive Filler Loaded Polysilazane-Derived Glass/Ceramic Coating Systems.....	18
M. Parchovianský / Passive filler loaded polysilazane-derived glass/ceramic coating system on AISI 441 stainless steel: Corrosion behaviour	20
A. Švančárková / Effect of Corrosive Media on Hardness and Wear resistance of Li₂Si₂O₅ glass-ceramics	22
J. Vráblová / Corrosion of IZOMER TT Glass Fiber Under Static Conditions In Distilled Water And In Borate Coolant Solution	24
O. Nowicka / Corrosion of 3Y-TZP ceramics for dental applications	26
A. Plško / Crystallisation of TiO₂ Xerogel.....	30
H. El-Maghraby / Solid-state fabrication of transparent YAG ceramics for optical applications: Characterization mixing, and processing of the starting oxides.....	31
P. Švančárek / White light emitting Y₂O₃ based fluorescents doped by ZnO	33
J. J. Velázquez García / From Xerogels to Aerogels: synthesis of porous oxyfluoride glass-ceramics for optical applications	36
M. Chromčíková / Structural relaxation of PbO-WO₃-P₂O₅ glasses.....	38
B. Hruška / Surface active components of glass forming melts identified by thermodynamic model	39
A. Prnová / HP sintering of yttrium-aluminate glass-Impact of particle size distribution on mechanical properties.....	41
M. Michálková / Preparation of YAG glass from glass microspheres	43
M. Hujová / Vitrification and upcycling of inorganic waste	45
K. Faturíková / Dielectric properties of Barium Crystal Galss	47
J. Michálková / Chemical Durability of Glass Fibres Insulation used in Nuclear Power Plants.....	49
Nibu G. P. / Characterization of Ce-doped yttria ceramics prepared by pressure filtration	51

Development of 3D Bioactive Silicate Based Glass-Ceramic Scaffolds with Hierarchical Porosity by Additive Manufacturing

Arish Dasan^a, Hamada Elsayed^{b,c}, Jozef Kraxner^a, Dusan Galusek^d, Enrico Bernardo^{*c}

^aDepartment of Glass Processing, FunGlass, Alexander Dubček University of Trenčín, Študentská 2, 911 50 Trenčín, Slovakia

(E-mail:arish.dasan@tnuni.sk)

^bCeramics Department, National Research Centre, Cairo, Egypt

^cDepartment of Industrial Engineering, Università degli Studi di Padova, Padova, Italy

^dJoint glass centre of the IIC SAS, TnUAD, and FChFT STU, FunGlass, Alexander Dubček University of Trenčín, Trenčín, Slovakia

ABSTRACT

Due to their excellent bioactivity and biocompatibility, silicate based biomaterials have received much attention in bone tissue engineering. Bone Implants for bone regeneration ideally need highly porous scaffolds, pore interconnectivity, optimized mechanical strengths and adaptable manufacturing. While it is challenging to produce complex porous ceramic components via conventional shaping methods, additive manufacturing enables to fabricate such components.

Silicones are a class of preceramic polymers, also known as polymer derived ceramics (PDCs), which can yield SiO₂ upon thermal treatment in air. Mixing silicones with active fillers leads to silicate based, bioactive, polymer derived glass-ceramics. For example, well known bioactive akermanite (Ca₂MgSi₂O₇) ceramic foams were developed from a liquid silicone mixed with CaO and MgO precursors by firing at 1100 °C. Intensive foaming was caused by water evaporation due to the decomposition of the fillers Mg(OH)₂ and hydrated borax as extra filler (which also formed liquid phase upon firing; led nearly phase pure components) at ca. 300-350 °C before firing at 1100 °C. It should be noted that the obtained akermanite ceramics by PDCs route did not compromise its biological responses. The advantage of PDCs route is not limited to shaping possibilities ((porous scaffolds could be shaped with silicone polymers before ceramization occurs); but also desirable ceramics could be obtained relatively low temperature than conventional methods. In addition, the low cost, easy handling and commercially available raw materials are also advantages. This characteristic property has recently provoked the use of preceramic polymers with reactive fillers in additive manufacturing technologies.

Direct ink writing (DIW) is an additive manufacturing technique that can be used to form green bodies via layer-by-layer extrusion of viscous pastes. Generally, in order to produce ceramic pastes, it needs sacrificial organic binder (during heat treatment binder will completely burn out), while silicone polymers can act as nonsacrificial binder as it yield one of the reactant upon heat treatment, to produce ceramic phases of a targeted composition when mixed with fillers.

The research here presented was essentially aimed at producing reticulated akermanite scaffolds, by direct ink writing of a paste consisting of silicone resins with CaO and MgO precursors, and with the additional constraint of forming porous struts, that would favour the impregnation with body fluids and cell adhesion. Despite scaffolds exhibited numerous cracks, due to the gas release from silicone resin and CaCO₃ upon heating, crack-free scaffolds with dense and regular struts were achieved by using addition of small amount (1.5 wt%) of anhydrous sodium borate (Na₂B₄O₇). On the contrary, scaffolds with homogenous 'spongy' struts were obtained by using hydrated sodium borate. No cracks were observed even in the latter case, owing to water vapour release at low temperature, before ceramic conversion. Both type of scaffolds (with dense or porous struts) exhibited remarkable (compressive strength of 7.3±1.1 MPa and 4.1±0.3 MPa with porosity 56.6 ± 2.6% and 68.7 ± 0.8%, respectively) strength-to-density ratios.

Keywords: Polymer derived glass ceramics; preceramic polymers; additive manufacturing; akermanite; direct ink writing; scaffolds.

References:

- [1] Bernardo E, Carlotti JF, Dias PM, Fiocco L, Colombo P, Treccani L, Hess U and Rezwani K, Novel akermanite-based Bioceramics from preceramic polymers and oxide fillers. *Ceram Int.* 2014;40:1029–1035.
- [2] Fiocco L, Li S, Stevens MM, Bernardo E, Jones JR, Biocompatibility and bioactivity of porous polymer-derived Ca-Mg silicate ceramics. *Acta Biomater.* 2017;50:56–67.
- [3] Fiocco L, Elsayed H, Daguano JKMF, Soares VO, Bernardo E, Silicone resins mixed with active oxide fillers and Ca–Mg Silicate glass as alternative/integrative precursors for wollastonite–diopside glass-ceramic foams. *J. Non-Cryst. Solids.* 2015;416:44-49.

Acknowledgment:



This paper is a part of the dissemination activities of project FunGlass. This project has received funding from the European Union's Horizon 2020 research and innovation programme under grant agreement No 739566 and in the frame of the project Centre for Functional and Surface Functionalized Glass (CEGLASS), ITMS code is 313011R453, operational program Research and innovation, co-funded from European Regional Development Fund

Sol-gel derived Zn-doped mesoporous bioactive glasses for biomedical applications

Z. Neščáková¹, L. Liverani², K. Zheng², Martin Michálek¹, D. Galusek¹, A. R. Boccaccini²

¹ FunGlass - Centre for Functional and Surface Functionalized Glass, Alexander Dubček University of Trenčín, Slovakia

(E-mail: zuzana.nescakova@tnuni.sk)

² Institute of Biomaterials, Department of Materials Science and Engineering, University of Erlangen-Nuremberg, Germany

Bioactive glasses (BG) continue to attract interest for applications in bone tissue engineering because of their bioactive, osteoconductive and osteoinductive properties. Their application possibilities have covered also the area of soft tissue engineering and wound healing (1). The discovery of mesoporous bioactive glasses (MBGs) opened a new direction for developing multifunctional bioactive materials by applying nanotechnology in regenerative medicine (2, 3). The main goal of the present work is the characterisation of SiO₂-CaO (MBG) and SiO₂-CaO-ZnO (MBG_Zn) bioactive glasses produced by the sol-gel route. The main feature of these nanosized SiO₂-based MBGs is the presence of a highly ordered mesoporous channel structure. The size of dispersed, spherical particles was in the range of 130 ± 10 nm. To connect the regenerative properties of MBGs with the beneficial effect of zinc, MBG doped with Zn²⁺ ions were successfully produced by using microemulsion assisted sol-gel method. EDS analyses and ICP_OES confirmed the presence of zinc in amount ~ 9 mol %. The designed material showed sustained released of zinc ions up to 21 days, reaching its maximum values after 14 days (1,12 mg/L). Cell culture tests with ST-2, MEF and MG-63 cell lines confirmed the cytocompatibility of the tested materials. SEM, XRD and FTIR indicated the formation of hydroxyapatite on the surface of MBG nanoparticles upon 3 days of immersion in simulated body fluid (SBF). On the other hand, the *in vitro* mineralization of MBG_Zn was markedly delayed confirming the same trend already reported in literature (4, 5) This fact can be considered an advantage in some applications such as wound dressing. These positive results confirm the suitability of the obtained MBG as candidates for biomedical applications.

Acknowledgement:



This paper is a part of the dissemination activities of project FunGlass. This project has received funding from the European Union's Horizon 2020 research and innovation programme under grant agreement No 739566 and in the frame of the project Centre for Functional and Surface Functionalized Glass (CEGLASS), ITMS code is 313011R453, operational program Research and innovation, co-funded from European Regional Development Fund.

References:

1. Míguez-Pacheco, V.; Hench, L.L.; Boccaccini, A.R. Bioactive glasses beyond bone and teeth: Emerging applications in contact with soft tissues. *Acta Biomater.* **2015**, *13*, 1-15.
2. X. Yan, C. Yu, X. Zhou, J. Tang, D. Zhao, Highly ordered mesoporous bioactive glasses with superior *in vitro* bone-forming bioactivities, *Angew. Chem. Int. Ed. Engl.* **2004**, *43*, 5980-5984.
3. Ch. Wu, Chang J., Multifunctional mesoporous bioactive glasses for effective delivery of therapeutic ions and drug/growth factors, *J. Con. Rel.* **2014**, *193*, 282-295.
4. Pérez, R.; Sanchez-Salcedo, S.; Lozano, D.; Heras, C.; Esbrit, P.; Vallet-Regí, M.; Salinas, A.J. Osteogenic effect of ZnO-mesoporous glasses loaded with osteostatin. *Nanomaterials* **2018**, *8*, 3-18.
5. Balasubramanian, P.; Strobel, L.A; Kneser, U.; Boccaccini, A.R. Zinc-containing bioactive glasses for bone regeneration, dental and orthopedic applications. *Biomed. Glasses* **2015**, *1*, 51-69.

Magnetic Mesoporous Silica Nanocomposites based on SBA-15/Fe₃O₄ as Multifunctional Nanoplatfoms for Technological Applications

Zulema Vargas-Osorio^{1,2}

¹Dpt. Biomaterials, FunGlass, Alexander Dubček University of Trenčín, Študentská 2, 911 50 Trenčín, Slovakia.
(E-mail:zulema.vargas@tnuni.sk),

²Departamento de Física Aplicada, Facultade de Física, Laboratorio NANOMAG, Instituto de Investigacións Tecnolóxicas, Universidade de Santiago de Compostela, E-15782, Santiago de Compostela, España.

ABSTRACT

Magnetic-mesoporous silica nanocomposite materials are emerging as one of the most appealing candidates to produce novel nanodevices with superior textural and magnetic properties. Their use as catalysts, adsorbents, gas storage and sensors have gained increasing importance¹. Particularly in biomedicine, their applications include MRI, magnetic hyperthermia, controlled drug release, bone tissue engineering, theranostics² and local cancer treatment³. These nanocomposites possess outstanding combined features providing a multifunctional activity⁴. On the one hand, SBA-15 mesoporous silica has a flat two-dimensional hexagonal symmetry with an ordered cylindrical pore channels system, which are highly interconnected. Moreover, SBA-15 shows remarkable hydrothermal and chemical stability, making it suitable for hosting and protecting important sensible molecules such as DNA, genes, enzymes, etc. Its surface plenty of silanol groups confers the ability of being easily modified by using organosilane species. On the other hand, the incorporation of superparamagnetic iron oxide nanoparticles (SPIONs) add different beneficial effects related to their nanosize and magnetic properties like magnetic stimulation on biological media (i.e., enhancement of cell adhesion, proliferation and differentiation), localized heat release by magnetic hyperthermia⁵, reinforcement of the SBA-15 mechanical properties. Besides, the presence of SPIONs confer the nanocomposites the capacity to be magnetically recovered from different environments as well as function as catalyst for Fenton reaction that can be used to degrade pollutants.

In this talk, different magnetic mesoporous materials^{4,6}, obtained by optimized synthetic methods and different in situ or ex situ approaches of magnetic doping, with chemically tailored morphological, textural and magnetic responses will be presented. TEM images of figures 1A and 1B display two different examples of magnetic mesoporous nanocomposites, where the magnetic nanoparticles are attached to the external silica surface, showing that they conserve the morphology and hexagonal symmetric disposition as their SBA-15 mesoporous silica precursor. N₂ adsorption analysis reveals surface areas above 200 m²/g, which are higher than those of conventional ceramics, ensuring an enhanced capacity for loading a large amount of molecules of different nature. XRD patterns reveal the conventional reflections associated with the SBA-15 type materials (low angle) as well as the presence of crystalline magnetite in these nanocomposites (figure 2A and 2B). The magnetization cycles show no hysteresis or coercive forces (figure 3), which is highly desirable for several applications to avoid magnetic agglomeration of particles. In addition, hyperthermia characterizations have been performed to assess the magneto-thermal abilities of some representative samples. The hyperthermia response can be tuned by varying both the content of magnetite and the location of magnetite on the (SBA-15/Fe₃O₄) composite system, as evidenced in figure 4. Negligible temperature increase (low magnetite content/magnetite inside SBA-15 mesopores) or a high increase of about 40° C in only one minute (high magnetite content/magnetite attached to external SBA-15 surface) can be obtained. Finally, the easiness of having organically modified surfaces with different functional groups provide them additional properties and features by incorporating, for example, fluorescent-labeling and antibody-bioconjugation.

Keywords: Magnetic mesoporous nanocomposites, magnetite, multiples functionalities, outstanding features, SBA-15, several applications.

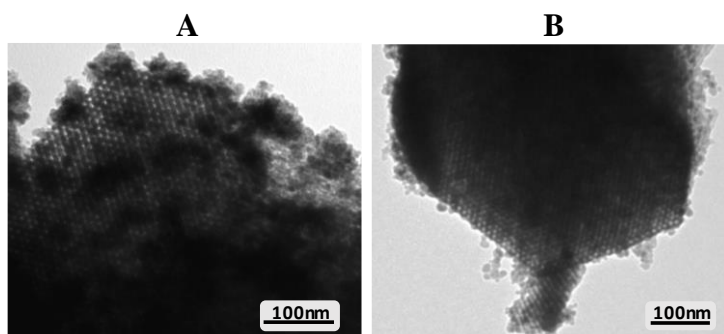


Figure 1. TEM images of the magnetic mesoporous nanocomposites A) Magnetic aggregates ($\text{Fe}_3\text{O}_4@\text{C}$) attached to external SBA-15 surface B) Magnetic NPs ($\text{Fe}_3\text{O}_4@\text{SiO}_2$) attached to external SBA-15 surface.

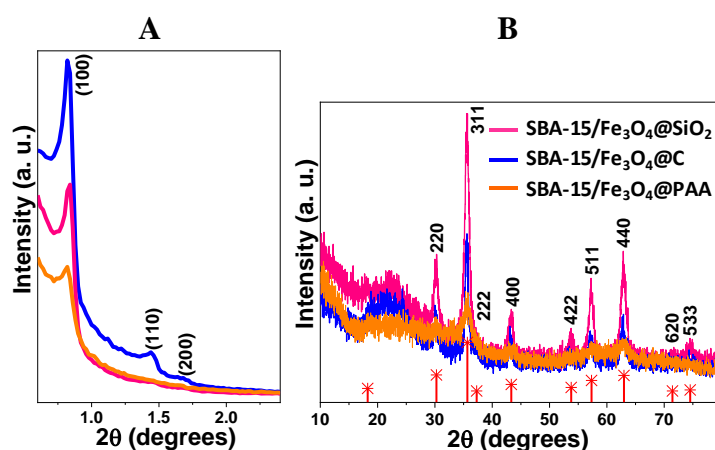


Figure 2. A) Low-angle XRD patterns and B) XRD patterns of the magnetic mesoporous nanocomposites. The expected peaks for magnetite (JCPDS card No. 19-0629) are also indicated at the bottom of the figures and the different peaks have been labelled with their corresponding Miller indexes.

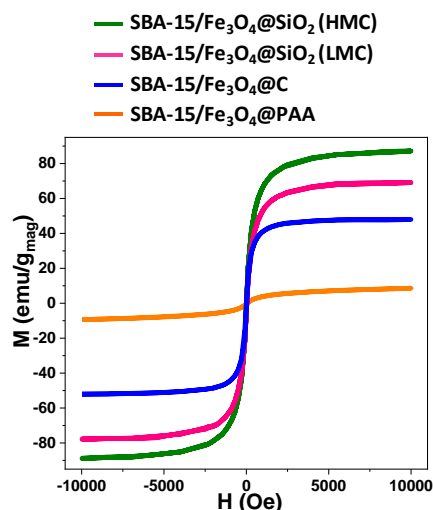


Figure 3. Hysteresis loops of the magnetic mesoporous nanocomposites up to 10 kOe. HMC = High magnetite content LMC = Low magnetite content

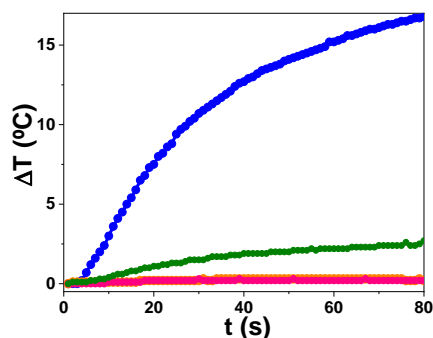


Figure 4. Heating curves of the magnetic mesoporous nanocomposites.

Acknowledgment:



This paper is a part of dissemination activities of project [FunGlass](#). This project has received funding from the European Union's Horizon 2020 research and innovation programme under grant agreement No 739566.

References:

- ¹ John Mondal, Tapas Sen and Asim Bhaumik. Fe_3O_4 @mesoporous SBA-15: a robust and magnetically recoverable catalyst for one-pot synthesis of 3,4-dihydropyrimidin-2(1H)-ones via the Biginelli reaction. *Dalton Trans.*, **2012**, 41, 6173–6181
- ² Zulema Vargas-Osorio, Andrés Da Silva-Candal, Yolanda Piñeiro, Ramón Iglesias-Rey, Tomas Sobrino, Francisco Campos, José Castillo and José Rivas. Multifunctional Superparamagnetic Stiff Nanoreservoirs for Blood Brain Barrier Applications. *Nanomaterials* **2019**, 9, 449; doi:10.3390/nano9030449
- ³ Vallet-Regí, María, and Eduardo Ruiz-Hernández. Bioceramics: from bone regeneration to cancer nanomedicine. *Advanced Materials* **23.44 (2011)**: 5177–5218.
- ⁴ Z. Vargas-Osorio, M. A. González-Gómez, Y. Piñeiro, C. Vázquez-Vázquez, C. Rodríguez-Abreu, M. A. López-Quintela and J. Rivas. Novel synthetic routes of large-pore magnetic mesoporous nanocomposites (SBA-15/ Fe_3O_4) as potential multifunctional theranostic nanodevices. *J. Mater. Chem. B*, **2017**, 5, 9395-9404.
- ⁵ Manuel Bañobre-López, Yolanda Piñeiro-Redondo, Monica Sandri, Anna Tampieri, Roberto De Santis, Valentin Alek Dediu, and José Rivas. Hyperthermia Induced in Magnetic Scaffolds for Bone Tissue Engineering. *IEEE TRANSACTIONS ON MAGNETICS*, VOL. 50, NO. 11, NOVEMBER **2014**.
- ⁶ Z. Vargas-Osorio, Y. Piñeiro, C. Vázquez-Vázquez, C. Rodríguez-Abreu, M. A. Álvarez-Pérez, M. A. López-Quintela and J. Rivas. Magnetic nanocomposites based on mesoporous silica for biomedical applications. *International Journal of Nanotechnology*. Vol. 13, No. 8, **2016**. DOI: 10.1504/IJNT.2016.079668.

Production of SiOC Based Bioactive Glass for Bone-Tissue Applications

Fulden Dođrul¹, Enrico Bernardo², Aldo R. Boccaccini³, Duřan Galusek⁴

¹ Department of Biomaterials, Centre for Functional and Surface-Functionalized Glasses, Alexander Dubcek University of Trencin, Trencin, Slovakia
(E-mail: fulden.dogrul@tnuni.sk)

² Department of Industrial Engineering, University of Padova, Via Marzolo 9, Padova, Italy

³ Institute of Biomaterials, Department of Materials Science and Engineering, University of Erlangen Nuremberg, CauerstraÙe 6, Erlangen, Germany

⁴ Joint glass centre of the IIC SAS, TnUAD, and FChFT STU, FunGlass, Alexander Dubcek University of Trencin, Trencin, Slovakia

ABSTRACT

Bioactive glass and glass ceramics are suitable materials for biomedical applications due to their ability to form normal tissue at their surfaces. In addition, they are able to establish a contiguous interface able to support the loads occurring at the site of implantation. From the point of view bio-applications, an ideal scaffold for bone regeneration must possess some characteristics, such as being bioactive and biocompatible, having controllable degradation rate in human body, and having similar mechanical properties to those of host bone. However, bioactive glass and glass ceramics are brittle. Due to insufficient mechanical properties they cannot be used alone for producing scaffolds for bone replacement and regeneration. Human bones also possess hierarchically organized porous structure. In order to mimic natural bone structure, scaffolds should be composed of interconnected highly porous network with appropriate pore structure, with the pore size supporting cell growth and transport of nutrients and metabolic waste. Even though there is a lot of reports related to improved structural properties of scaffolds for bone-tissue engineering, the problem related to adjusting the balance between mechanical properties and required porosity remains unresolved^{1,2,3}.

In 2016 Riedel et al. reported on bioactivity of silicon oxycarbide-based (SiOC) glass. Silicon oxycarbide (SiOC) based glass refers to carbon-containing silicate glass where silicon atoms bond to carbon and oxygen atoms in an amorphous network. The network of silicon oxycarbide glass is formed by corner-shared silicon-centered tetrahedra comprising Si-O and Si-C bonds, but not C-O bonds (SiO_xC_{4-x} tetrahedra). The structure therefore consists of mixed bonded SiO_xC_{4-x} tetrahedra (i.e., SiO₄, SiO₃C, SiO₂C₂, SiOC₃, and SiC₄) instead of separate mixture of intergrown silicon carbide and silicon oxide nanophases. The presence of carbon in the silicate glasses increases bonding per anion by replacing two coordinated oxygen with four coordinated carbon. Due to increased bonding, molecular structure of glass network is strengthened and its thermal and mechanical properties are improved^{4,5}.

Silicate based materials, because of its sintering difficulties, generally are obtained by using hydrothermal method, spark plasma-sintering, solution combustion processes and sol-gel processing. It can be said that sol-gel method is the most suitable way for the preparation of complex structures due to possibility of exact stoichiometry control. Even though this method has several advantages, it is hard to transfer it to industry, especially in terms of production of bulk components because of the cost of the raw materials, the presence of large amounts of solvents and the associated drying problems. Compared to sol-gel method, preceramic polymer fabrication avoids problems with drying, processing time is shorter, and allows processing in molten state. Moreover, commercially available siloxanes, as the most important raw materials for production of SiOC glass are relatively cheap and do not require specialized handling procedures. Using preceramic polymers give rise to important technological advantages^{6,7}.

The aim of the present study is to overcome the mechanical drawbacks of bioactive glasses by utilizing SiOC based glass and glass-ceramics prepared from preceramic polymers and at the same time to enhance the bioactivity of these materials. Effect of dopants like MgO, CaO and NaO will be studied with the aim to enhance the bioactivity of these materials, as required for bone tissue engineering applications. Fabrication of various structures in the form of tablets, foams and 3D printed scaffolds will be utilized.

Keywords: Silicon oxycarbide, Black glass, Pre ceramic polymer, Bone tissue engineering, Additive manufacturing

Acknowledgment:



This paper is a part of dissemination activities of project [FunGlass](#).

This project has received funding from the European Union's Horizon 2020 research and innovation programme under grant agreement No 739566.

Financial support of this work by the grant SAS-MOST JRP 2018/2 is gratefully acknowledged.

References:

1. Kargozar S, Mozafari M, Hamzehlou S, Brouki Milan P, Kim H-W, Baino F. *Bone Tissue Engineering Using Human Cells: A Comprehensive Review on Recent Trends, Current Prospects, and Recommendations*. Vol 9.; 2019. doi:10.3390/app9010174
2. Riches P, Jia L, Turnbull G, et al. Bioactive Materials 3D bioactive composite scaffolds for bone tissue engineering d e. 2018;3:278-314. doi:10.1016/j.bioactmat.2017.10.001
3. Jones JR. Bioactive Glass 3D Scaffolds for Tissue Engineering. 2002;(September).
4. Gonzalo-Juan I, Detsch R, Mathur S, Ionescu E, Boccaccini AR, Riedel R. Synthesis and in vitro activity assessment of novel silicon oxycarbide-based bioactive glasses. *Materials (Basel)*. 2016;9(12):1-11. doi:10.3390/ma9120959
5. Stabler C, Ionescu E, Gonzalo-juan I, Graczyk-zajac M. Silicon Oxycarbide Glasses and Glass-Ceramics : “ All-Rounder ” Materials for Silicon oxycarbide glasses and glass - ceramics : “ All - Rounder ” materials for advanced structural and functional applications. 2018;(August). doi:10.1111/jace.15932
6. Colombo P, Mera G, Riedel R, Sorarù GD. Polymer-Derived Ceramics: 40 Years of Research and Innovation in Advanced Ceramics1). *Ceram Sci Technol Appl*. 2013;4:245-320. doi:10.1002/9783527631971.ch07
7. Pantano CG, Singh AK, Zhang H. Silicon oxycarbide glasses. *J Sol-Gel Sci Technol*. 1999;14(1):7-25. doi:10.1023/A:1008765829012

Synthesis of Cerium and Gallium Doped Mesoporous Bioactive Glass Nanoparticles

Fatih Kurtuldu¹, Dušan Galusek² and Aldo R. Boccaccini³

¹ Department of Biomaterials, FunGlass, Alexander Dubcek University in Trencin, Slovakia
(E-mail: fatih.kurtuldu@tnuni.sk)

² Joint Glass centre of the IIC SAS, TnUAD and FChFT STU, FunGlass, Trencin, Slovakia

³Institute of Biomaterials, University of Erlangen-Nuremberg, Germany

ABSTRACT

According to the IUPAC definition, porous materials are divided into three classes: microporous (pore size < 2 nm), mesoporous (2–50 nm) and macroporous (>50 nm) [1]. Ordered mesoporous silica was first discovered in 1992 [2], and proposed as a drug delivery system in 2001 [3]. Since then silica-based glass microspheres, such as MCM-41, SBA-15 or MCM-48 representing ordered mesoporous inorganic materials, have been considered as ideal materials for incorporation of drugs, genes and other therapeutic agents acting as carrier and control release systems. In this study, the synthesis of mesoporous bioactive glass nanoparticles, consisting of a silicate network modified by Ca and Ce or Ga ions, has been studied for possible applications in cancer treatment or incorporation into nanocomposite scaffolds for bone regeneration.

Tetraethylorthosilicate (TEOS, 100%, VWR International), hexadecyltrimethylammonium bromide (CTAB, BioXtra, ≥99%, Sigma-Aldrich), ethyl acetate (99.7%, Centralchem), ammonium hydroxide (ACS reagent, 28.0 - 30.0% NH₃ basis, Sigma-Aldrich), Cerium nitrate hexahydrate (99.95%, Treibacher) and gallium nitrate hexahydrate (99.999%, Alchemica) were used as starting materials for synthesis of mesoporous bioactive glass nanoparticles (MBGNPs).

Cerium doped mesoporous bioactive glass nanoparticles (MBGNPs) in the 60SiO₂-(40-x)CaO-xCe₂O₃ system and gallium doped MBGNPs in the 60SiO₂-(40-x)CaO-xGa₂O₃ system, where x stands for 0, 1, 3 and 5 mole %, were obtained by micro-emulsion assisted sol-gel method. First, 2.8 g of CTAB templating agent was dissolved in 150 mL deionized water, and 40 ml of ethyl acetate was added. Ammonium hydroxide (3.66 ml) was then added and mixed at room temperature. TEOS (14.4 ml) and appropriate quantities of calcium nitrate tetrahydrate, cerium nitrate hexahydrate or gallium nitrate hexahydrate were added step wise to the solution within a 30 minutes time interval, and the solution was left for 4 hours. Afterwards the precipitates were filtered and washed with deionized water and EtOH to remove unreacted precursors and remaining salts, and dried at 60°C overnight. Finally, the dried samples were thermally treated at 650 °C/3 h (heating rate 1 °C min⁻¹) to remove the surfactant and nitrate groups and to stabilize the glassy phase.

Micro-emulsion assisted sol-gel method allowed the preparation of MBGNPs with spherical shape, monomodal size distribution with the mean equivalent diameter of 150 nm and a low degree of agglomeration. SEM micrographs and EDS spectra of undoped MBGNPs are shown in Fig. 1. The results of acid digestion method confirm that the glass nanoparticles contain 12.6 mol % CaO. The high resolution SEM micrographs revealed fine surface structure of the nanoparticles indicating their mesoporous structure.

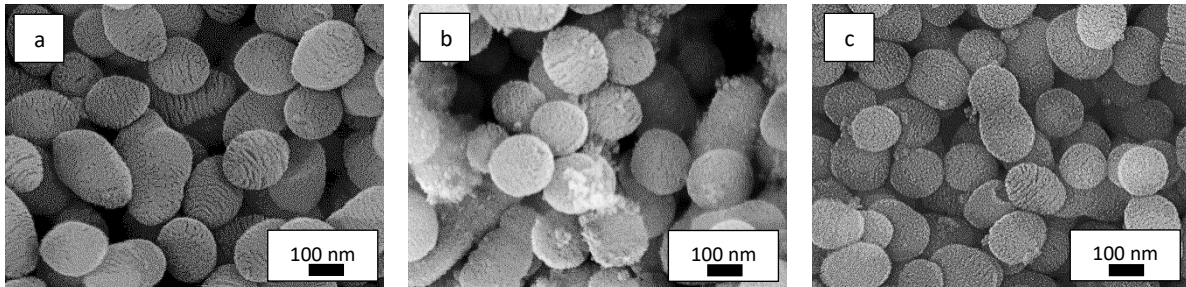


Figure 1 SEM images of a) undoped, b) doped with 1 mol% cerium and c) doped with 1 mol% gallium Mesoporous Bioactive Glasses produced by Micro-Emulsion Sol-Gel method.

Synthesis of nanoparticles with up to 1 mol% of Ce and Ga yielded nanoparticles of size, shape, and surface pore structure similar to those of the undoped MBGNPs. Increasing the content of dopants up to 3 and 5 mol % resulted in deformation of the spherical shape of the nanoparticles and yielded elongated pineal shaped particles with aspect ratio 5:3. In addition, calcium content decreased significantly (down to 4.4 mol% CaO for gallium and 0.7 mol CaO for cerium), most likely due to replacement of Ca in the glass structure with the ions of the dopants. The influence of doping on specific surface and mesoporosity of synthesized nanoparticles has been evaluated and critically discussed. Specific surface area increased with 1 mol% of doping, 345 m²/g to 412 m²/g for Ce and 486 m²/g for Ga. Increasing the content of dopants up to 3 and 5 mol% resulted in decreasing surface area and increasing the size of the mesoporous.

The micro-emulsion assisted sol-gel method yielded monodispersed mesoporous bioactive glass nanoparticles in the system CaO-SiO₂ doped with up to 5 mol % of Ce and Ga, and with low or no agglomeration. Incorporation of higher concentrations of dopants resulted in distortion of the MBGNPs spherical shape and marked decrease of Ca content. The influence of doping specific surface and mesoporosity of synthesized nanoparticles has been studied.

Keywords: Bioactive glass, Cerium, Gallium, Micro-emulsion, Nanoparticles

Acknowledgment:



This paper is a part of dissemination activities of project [FunGlass](#). This project has received funding from the European Union's Horizon 2020 research and innovation programme under grant agreement No 739566. Financial support of this work by the grant SAS-MOST JRP 2018/2 is gratefully acknowledged.

References:

- [1] K. S. W. Sing, "Reporting physisorption data for gas/solid systems with special reference to the determination of surface area and porosity (Recommendations 1984)," *Pure Appl. Chem.*, vol. 57, no. 4, pp. 603–619, 1985.
- [2] C. T. Kresge, M. E. Leonowicz, W. J. Roth, J. C. Vartuli, and J. S. Beck, "Ordered mesoporous molecular sieves synthesized by a liquid-crystal template mechanism," *Nature*, vol. 359, no. 6397, pp. 710–712, 1992.
- [3] M. Vallet-Regi, A. Rámila, R. P. Del Real, and J. Pérez-Pariente, "A new property of MCM-41: Drug delivery system," *Chem. Mater.*, vol. 13, no. 2, pp. 308–311, 2001.

Incorporation of Zinc Doped Borate Bioactive Glasses into Soft Matrices for Wound Healing Applications

Nurshen Mutlu¹, Hana Kankova², Dagmar Galuskova², Dušan Galusek³, and Aldo R. Boccaccini⁴

¹ Department of Biomaterials, FunGlass, Alexander Dubcek University, Trencin, Slovakia
(E-mail: nurshen.mutlu@tnuni.sk)

² FunGlass, Alexander Dubcek University, Trencin, Slovakia

³ Joint glass centre of the IIC SAS, TnUAD and FChFT STU, FunGlass, Alexander Dubcek University, Trencin, Slovakia

⁴ Institute of Biomaterials, Friedrich–Alexander University Erlangen–Nürnberg, Germany

ABSTRACT

Application of bioactive glasses in orthopedic and dental application, as well as bone tissue engineering gained a great interest in the last 50 years since its discovery by Hench et al. in 1971 [1]. Most frequently studied and well documented system for bone filling materials, dental application and bone implants bioglass are the compositions 45S5 (45% SiO₂, 24.5% Na₂O and CaO, 6% P₂O₅ by wt.) and 13-93 (53% SiO₂, 20% CaO, 12% K₂O, 6% Na₂O, 5% MgO, 4% P₂O₅). Recently boron containing glasses attracted attention for applications beyond bone and teeth: soft tissue applications including wound healing are also studied. Bioactive borate glasses show 5 times faster biodegradation and better bioactivity compare to silicate glass due to presence of silicate-rich layer [2]. Unlike the 45S5 silicate bioactive glass, they transform to hydroxyapatite (HA) completely. This feature originates from less stable structure of boron containing glasses with different type of glass forming units and lower network connectivity [3]. When considering all these properties, borate bioactive glasses can be pointed out as promising biomaterials for wound healing applications.

To provide ideal dressing for a wound, both natural environment and healing process needs to be mimicked. For this purpose, both natural and synthetic polymers can be applied. However, the polymers by themselves are insufficient in providing required mechanical strength, chemical reactivity, biocompatibility and bioactivity to mimic natural tissue. Their mechanical properties must be improved and optimized, and additional bioactivity must be provided by another component [4]. Borate glasses are one of the promising candidates for preparation of a biocomposite material which could provide temporary support for new tissue formation.

When the body cannot heal naturally, suitable stimulation is needed to enhance the healing process. This can be achieved by the use of biomaterials, which release suitable ions such as Ca, P, B etc. to the surrounding area. These ions have specific roles during hemostasis, inflammation, proliferation and tissue remodelling phases of wound healing. For example, Ca ions that is present in a BG composition as a glass modifier, can promote the migration of epidermal cells and accelerate formation of blood clot. Upon dissolution, silicate and borate bioactive glasses increase the local pH contributing to antibacterial effect. Bioactive glasses can be also doped with therapeutic ions such as Ag⁺, Cu²⁺, Ga³⁺ and Zn²⁺ with antibacterial properties, thus assisting and promoting the wound healing process[5].

In this study, 1393-B3 bioactive glass doped with zinc was produced by conventional melting. The compositions of prepared glasses are summarized in Table 1. In doped glasses Zn was added to substitute calcium. The real composition of prepared glasses was verified by chemical analysis by optical emission spectroscopy in inductively coupled plasma (ICP-OES, VARIAN MPX), (Table 2). The real compositions of produced glass corresponds with the theoretical compositions. The X-ray powder diffraction data (2 θ , range from 10 to 80), confirmed that produced bioactive zinc doped glasses were X-ray amorphous (Fig.1.).

Table 1. Composition of produced borate bioactive glasses

Mol%	1393B3	1Zn-1393B3	3Zn-1393B3	6Zn-1393B3
Na ₂ O	5.96	5.96	5.96	5.96
K ₂ O	7.91	7.91	7.91	7.91
MgO	7.66	7.66	7.66	7.66
CaO	22.15	21.15	19.15	16.15
B ₂ O ₃	54.75	54.57	54.57	54.57
P ₂ O ₅	1.75	1.75	1.75	1.75
ZnO	-	1	3	6

Table 2. ICP-OES result of produced bioactive borate glasses

Mol %	B ₂ O ₃	K ₂ O	MgO	Na ₂ O	CaO	P ₂ O ₅	ZnO
1393-B3	52.76±0.76	10.55±0.18	3.97±0.07	4.17±0.07	17.83±0.2	3.50±0.05	-
1Zn	51.51±1.42	10.25±0.28	4.15±0.10	4.06±0.09	17.34±0.4	3.55±0.12	1.10±0.02
3Zn	50.49±0.16	10.11±0.051	3.93±0.02	3.91±0.01	14.83±0.08	3.37±0.04	3.23±0.01
6Zn	52.40±3.03	10.93±0.17	4.28±0.04	4.21±0.09	13.80±0.40	3.70±0.11	7.16±0.16

Future work will include the studies of bioactivity and degradation of zinc doped glasses. In addition, Ga-doped borate bioactive glasses will be produced by conventional glass melting route and will be characterized in the same manner. Biocomposite fibres containing Ga and Zn doped bioactive borate glasses in polylactic acid polymeric matrix will be produced by electrospinning method as potential dressings for wound healing applications.

Keywords: Biocomposite, bioactive borate glass, wound healing.

Acknowledgment:



This paper is a part of dissemination activities of project [FunGlass](#).

This project has received funding from the European Union's Horizon 2020 research and innovation programme under grant agreement No 739566.

Financial support of this work by the grant SAS-MOST JRP 2018/2 is gratefully acknowledged

References:

- [1] L.L. Hench, R.J. Splinter, W.C. Allen, T.K. Greenlee, Bonding mechanisms at the interface of ceramic prosthetic materials, *J. Biomed. Mater. Res.* 5 (1971) 117–141. doi:10.1002/jbm.820050611.
- [2] A.R. Boccaccini, of Angiogenic potential of boron-containing bioactive glasses : in vitro study, (2017) 8785–8792. doi:10.1007/s10853-016-0563-7.
- [3] V. Miguez-Pacheco, L.L. Hench, A.R. Boccaccini, Bioactive glasses beyond bone and teeth: Emerging applications in contact with soft tissues, *Acta Biomater.* 13 (2015) 1–15. doi:10.1016/j.actbio.2014.11.004.
- [4] L. Gritsch, G. Conoscenti, V. La Carrubba, P. Noeaid, A.R. Boccaccini, Poly lactide-based materials science strategies to improve tissue-material interface without the use of growth factors or other biological molecules, *Mater. Sci. Eng. C.* (2018) 0–1. doi:10.1016/j.msec.2018.09.038.
- [5] S. Naseri, W.C. Lepry, S.N. Nazhat, Bioactive glasses in wound healing: Hope or hype?, *J. Mater. Chem. B.* 5 (2017) 6167–6174. doi:10.1039/c7tb01221g.

Magnetic Bioactive Materials for Bone Regeneration and Tissue Engineering

Susanta Sengupta¹, Martin Michalek¹, Dušan Galusek^{1,2}, Aldo R. Boccaccini³

¹ Department of Biomaterials, Centre for Functional and Surface Functionalized Glass, Alexander Dubcek University in Trenčín, Slovakia

² Joint glass centre of the IIC SAS, TnUAD and FChFT STU, FunGlass, Trenčín, Slovakia

³ Institute of Biomaterials, Department of Materials Science and Engineering, University of Erlangen-Nuremberg, Erlangen, Germany

Tissue Engineering is an interdisciplinary area that combines the concept of cell biology, drug delivery, materials science and engineering, which focused on the regeneration of specific cells and functional tissues. Depending on the scaffold materials cell growth or tissue regeneration can be efficient; cells can undergo attachment, growth, differentiation and proliferation on effective bioactive materials. Biomaterials like bioactive glass (45S5, 1393, 1393B3, 1393B1, 58S), ceramic materials (hydroxyapatite), glass-ceramics, biodegradable or biocompatible polymers are specially used for the preparation of such kind of scaffolds [1, 2]. Based on the nature of the used bioactive materials different processes and technologies are used for scaffold preparations, e.g. freeze casting, solvent casting, robocasting, foam replication method, 3D printing, electrospinning etc.

Bioactive glasses, especially 45S5, 1393, 1393B1, have been considered as a promising alternative in the treatment of bone related diseases, therapeutic ions (B, Cu, Zn, Mg, Co, Sr, Ca) doped glass scaffolds also have the ability to form bone minerals, like hydroxycarbonated apatite (HCA), after immersion in simulated body fluid (SBF). Mesoporous glass based materials prepared by sol-gel method are excellent materials with high specific surface area, and possess very high loading capacity for successful delivery of potential growth factors (proteins, enzymes, drugs etc.). Recent results indicate that magnetic field may stimulate the new tissue generation by enhancing the cell proliferation and differentiation process [3]. Magnetic fields were also found to be beneficial for promoting bone regeneration, integration of bone and implants, and increase of bone density [4]. For this purpose, magnetic force based tissue engineering has been reported that utilizes magnetic nanodevices (magnetic cationic liposomes, magnetic gelatine nanoparticles, magnetic nanoparticles loaded hydroxyapatite-collagen etc.) to yield magneto-responsive features to the cells [5].

However, a possibility that has rarely been considered is the application of magnetic nanoparticles in tissue regeneration, is their incorporation into scaffolds. The aim of this study is to combine the concept of biomaterials, especially bioactive glasses, and polymer materials with magnetic nanotechnology for efficient hard and soft tissue regeneration. For successful tissue regeneration some crucial factors should be maintained, such as the use of suitable non-toxic and biocompatible materials for scaffold preparation, culture medium, temperature and most important, cell numbers in scaffolds. The last factor is quite difficult to manage properly; magnetic force guided cell seeding can be applied to optimise the cell numbers in scaffolds. High cell number with sufficient packing of cells at the interior of the scaffold has been addressed by loading the cells with magnetic nanoparticles (magnetic cationic liposomes or chitosan-coated magnetic nanoparticles), hydrating the scaffold with the suspension of the cells and applying a magnetic field consequently [6]. Such kind of protocol can be productive for cell seeding into the deeper sites of the 3D porous scaffolds, which may not be possible in absence of external magnetic field. Thus, the magnetic field intensity has been found to have positive influence on the depth of the cell seeding into the scaffold [7]. After all mechanical stimuli similar to those experienced *in-vivo* by cells, couldn't provided to the seeded cells at the time of incubation on scaffold. Moreover, direct magnetic actuation can provide mechanical stimuli experienced by cells *in-vivo*, which can't be simulated by *in-vitro* tests in incubators. These are achieved through attachment of magnetic nanoparticles on specific ionic channels present on the cellular membrane, acting as stress generators [8]. It was demonstrated that mechanical stimulation of primary human osteoblast cells by attached

magnetic nanoparticles promoted the regeneration of bone matrix under the influence of external magnetic field [9].

Finally, our work relies on magnetic nanoparticles with therapeutic ions (Zn, B, and Ca) doped mesoporous glass-polymer fibre composites. Citrate stabilized superparamagnetic magnetite (Fe_3O_4) nanoparticles will be prepared by co-precipitation method [10]. Therapeutic ions doped mesoporous bioactive glass nanoparticles (MBGN) will also be prepared separately by sol-gel method [11]. These will be used for preparation of biocomposites. Poly-vinylpyrrolidone (PVP; a water soluble polymer) will be dissolved in water. Required amount of magnetic nanoparticles and mesoporous glass nanoparticles will be added to the polymeric solution and the whole mixture will be homogenized by ultrasonication. The PVP/ Fe_3O_4 /MBGN sol will be used for fibre drawing by electrospinning. Due to the presence of citrate groups at the surface the magnetite nanoparticles can be easily dispersed in aqueous polymeric solution. The presence of polymeric chains in the aqueous medium will also partly or completely eliminate interparticle attractive forces, thus preventing their aggregation.

Morphology of the final fibre mats will be studied by using a scanning electron microscope (SEM). Transmission electron microscope (TEM) is also be useful to study the distribution of MBGN (~150-180 nm) and magnetite nanoparticles (~ 10-20 nm) in fibres due to their different size range, and Energy dispersive X-ray spectroscopy (EDAX) for elemental distribution in the fibre. Magnetic properties of the fibres will be measured by a magnetometer at room temperature and finally the cell culture study will be done with different cell lines in cell culture medium (*in-vitro*). Based upon the results of the *in vitro* analysis, *in vivo* studies will be envisaged on selected fibre mats. The final objective is to evaluate the bioactivity of the magnetic bioglass-polymer fibre composites after implantation in the animal body.

Keywords: Tissue regeneration, Cell, Scaffold, Biomaterials, Magnetic Nanoparticles.



This paper is a part of dissemination activities of project [FunGlass](#). This project has received funding from the European Union's Horizon 2020 research and innovation programme under grant agreement No 739566.

References:

1. L. C. Gerhardt, A. R. Boccaccini. *Materials*. **2010**, 3 (7), 3867-3910.
2. A. R. Boccaccini, M. Erol, W. J. Stark, D. Mohn, Z. Hong, J. F. Mano. *Compos. Sci. Technol.* **2010**, 70 (13), 1764-1776.
3. J. Kanczler, J. Magnay, D. W. Green, R. O. C. Oreffo. *Tissue. Engg. Part-A*. **2010**, 16 (10), 3241-3250.
4. B. N. Luna, M. Sabanero, M. Sosa, M. A. Rodriguez. *Micron*. **2011**, 42, 600-607.
5. Y. Li, D. Ye, M. Li, M. Ma, N. Gu. *Chem. Phys. Chem.* **2018**, DOI:10.1002/cphc.201701294
6. K. Shimizu, A. Ito, H. Honda. *J. Biomed. Mater. Res., Part B: Appl. Biomater.* **2006**, 77B, 265.
7. Y. Gao, J. Lim, S. H. Teoh, C. Xu. *Chem. Soc. Rev.* **2015**, DOI: 10.1039/c4cs00322e
8. S. Gil, J. F. Mano. *Biomater. Sci.* **2014**, 2, 812-818.
9. S. H. Cartmell, J. Dobson, S. B. Verschuere, A. J. E. Haj. *IEEE Trans. Nano.biosci.*, **2002**, 1, 92-97.
10. A. Bee, R. Massart, S. Neveu. *J. Magn. Magn. Mater.* **1995**, 149, 6-9.
11. Q. Liang, Q. Hu, G. Miao, B. Yuan, X. Chen. *Materials Letters*. **2015**, 148, 45-49.

Sol-gel based hybrid coatings for corrosion protection of AA2024-T3 alloys

N. Afsharimani¹, Y. Castro², A. Duran² and D. Galusek¹

¹ Department of Coating Processes, FunGlass, Alexander Dubček University of Trenčín, Študentská 2, 911 50 Trenčín, Slovakia

(E-mail:nasima.afsharimani@tuni.sk)

² Departamento de Vidrios, Instituto de Cerámica y Vidrio (ICV), Consejo Superior de Investigaciones Científicas(CSIC), C/ Kelsen n° 5, Campus de Cantoblanco (UAM), 28049 Madrid, Spain

ABSTRACT

Hybrid sol-gel coatings were synthesized and studied in the present work as pre-treatments for the aluminum alloy AA2024-T3 to provide corrosion protection in 0.05 M NaCl solution. The pristine sol-gel films were prepared from Tetraethoxysilane (TEOS) and 3-glycidoxypropyltrimethoxysilane (GPTMS) precursors. The coatings synthesis protocol was further developed by incorporation of graphene nanosheets and colloidal SiO₂ nanoparticles with the aim of improving the structural properties such as coating integrity and barrier properties against corrosive medium. To this end, graphene nanosheets were modified through a straightforward hydrothermal approach which resulted in compatible and stable dispersion of nanosheets into GPTMS/TEOS sols (Fig.1). Additionally, the hybrid sols were doped with colloidal SiO₂ (Ludox) nanoparticles to achieve dense and defect free structures. Optimization of sol synthesis was based on the results of ATR-FTIR and UV-vis-NIR spectroscopies. Opening of epoxy rings and completion of hydrolysis and condensation reactions during the synthesis process were also confirmed. Coatings were characterized through thickness, water contact angle, and electrochemical properties (potentiodynamic polarization).

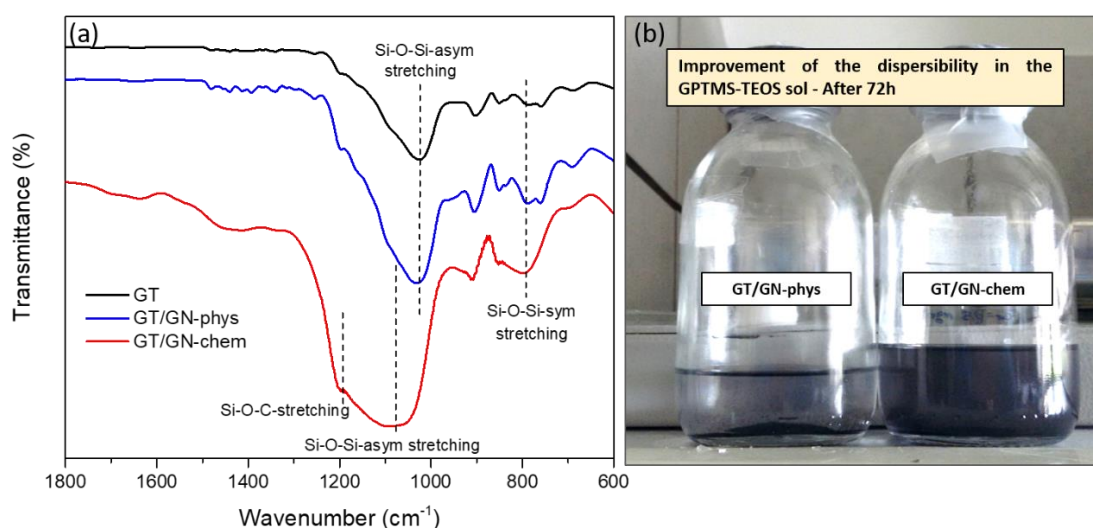


Fig. 1. (a) FTIR spectra of pristine GPTMS/TEOS (GT, black curve), GPTMS/TEOS doped with graphene nanosheets before chemical modification (GT/GN-phys, blue curve) and GPTMS/TEOS doped with chemically modified graphene nanosheets (GT/GN-chem, red curve) and (b) visual image of dispersion improvement of graphene nanosheets in GPTMS/TEOS sols after chemical modification.

The results showed that the incorporation of graphene nanosheets into hybrid sol-gel coatings affected the corrosion properties. According to surface chemical, structural and electrochemical characterizations, incorporation of chemically modified graphene nanosheets into TEOS and GPTMS sols including colloidal SiO₂ led to the better corrosion protection properties compared to those with graphene nanosheets embedded in pure TEOS and GPTMS sols. The coatings based on chemically modified graphene and SiO₂ nanoparticles appeared to be thicker (thickness = 5.5 ± 0.2 μm) and rougher (average roughness = 7.4 ± 0.1 nm) with reduced hydrophilicity (water contact angle = 74 ± 2 °). According to polarization measurements, promising passive (barrier) ranges were

formed for such coatings and corrosion current densities decreased down to values almost $\sim 10^5$ times smaller than that of the bare AA2024-T3 alloy (Fig.2). Such encouraging barrier properties could originate from the both layered graphene structure and the presence of SiO_2 nanoparticles that likely reduced the active surface area of the coating accessible for the attack of the corrosive medium through perhaps reinforcing the cross-linking density. These coatings could be promising candidates to be applied on the surface of AA2024-T3 alloys combined with deposition of an organic top coat for corrosion protection applications.

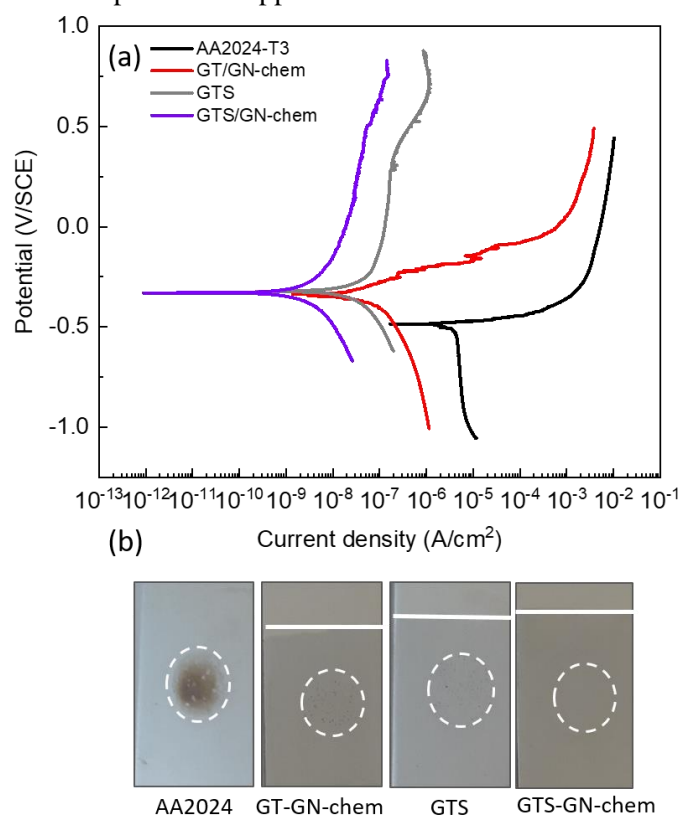


Fig. 2 (a) Potentiodynamic polarization curves of bare AA2024-T3 alloy (black curve) and samples coated with hybrid sol-gel coatings including GPTMS/TEOS doped with chemically modified graphene nanosheets (GT/GN-chem, red curve), GPTMS/TEOS/colloidal SiO_2 (GTS, grey curve) and GPTMS/TEOS/colloidal SiO_2 doped with chemically modified graphene nanosheets (GTS/GN-chem, purple curve) and (b) visual images of corroded surface areas (white dashed circles) after exposure to corrosive medium (0.05 M NaCl). For a better visibility, the white lines indicate the boarder between the coated and uncoated areas. As it is visible to the naked eye, the sample with GTS-GN-chem coating shows the least surface damage compared to the bare alloy.

Keywords: Aluminum alloy, Sol-gel coatings, Corrosion protection, Barrier properties, SiO_2 nanoparticles, Graphene nanosheets.

Acknowledgement:



This paper is a part of dissemination activities of project [FunGlass](#). This project has received funding from the European Union's Horizon 2020 research and innovation programme under grant agreement No 739566.

Inkjet printing of ceramic precursors based on sol-gel media

Zitnan Michal^{1,2}, Müller Lenka², Höppener Stephanie³, Galusek Dusan¹, Wondraczek Lothar²

¹ FunGlass, Alexander Dubcek University of Trencin, Studentska 2, 91150 Trencin, Slovakia
(E-mail: michal.zitnan@tnuni.sk)

² Friedrich Schiller University Jena, Otto Schott Institute of Materials Research, Fraunhoferstr 6, D-07743 Jena, Germany

³ Friedrich Schiller University Jena, JCSM, Philosophenweg 7, D-07743 Jena, Germany

ABSTRACT

This work focuses on direct inkjet printing of sol-gel-based precursors using commercially available and low-cost inkjet printer to print complex features with high spatial resolution. It allows to prototype fine structures like waveguides, biosensors or gas sensors [1]. This work demonstrates a new method of modifying the consumer inkjet printer to prepare ceramic layers on fused silica substrate. We re-engineered the printer by modifying the hardware, while preserving the printer's ability to be controlled by conventional software. The hardware upgrade enables fluid deposition on rigid substrates with the print accuracy and precision close to unmodified printer using thermal ink cartridges [2]. Although this method of printing promises high processing speeds, the performance of this process is often limited by the rheological parameters of the ink [3]. In our study, we focus on ceramic precursors prepared by various sol-gel routes [4]. One of the significant issues in printing is premature clogging of inkjet printheads when printing aqueous sols [5]. To avoid clogging on internal surfaces of the printhead a systematic design of inkjet inks is needed. The design must address ink rheology, colloidal stability and suppress cracks formation during firing. Water based inks with low viscosity and moderate surface tension were designed. The rheological properties of the ink have been determined by viscosity, surface tension and contact angle measurements. Proper control over rheology and surface tension resulted in good printability [6]. The quality of printed patterns like line stability, edge acuity and cross-section of the lines was characterized by using confocal optical microscopy. Drying of the precursor yields composite powders forming mullite structure after firing at 1300°C, as confirmed by X-ray powder diffraction before realizing the inkjet printing. Proper adjustment of quantities of each component and processing conditions resulted in preparation of stoichiometric $3\text{Al}_2\text{O}_3 \cdot 2\text{SiO}_2$ mullite layer in one step process.

Keywords: Ceramic coatings, Design of the ink, Inkjet printing, Mullite, Re-engineering of the printer, Sol-gel

Acknowledgment:



This paper is a part of dissemination activities of project [FunGlass](#).

This project has received funding from the European Union's Horizon 2020 research and innovation programme under grant agreement No 739566 and in the frame of the project Centre for Functional and Surface Functionalized Glass (CEGLASS), ITMS code is 313011R453, operational program Research and innovation, co-funded from European Regional Development Fund.

References:

- [1] Li, T., Dong, Y., Yuan, D., Liu, Y. *AIP Advances* **5** (2015) 041327
- [2] Orloff N.D. et al. *RCS Adv.* **4** (2014) 34721-34728

- [3] Nallan, H.C., Sadie, J.A., Kitsomboonloha, R., Volkman, S.K., Subramanian, V. *Langmuir* **30** (2014) 13470-13477
- [4] Cividanes, L.S., Campos, T.M.B., Rodrigues, L.A., Brunelli, D.D., Thim, G.P. *J. Sol-Gel Sci Technol* **55** (2010) 111-125
- [5] Li Y., Dahhan, O., Filipe, C.D.M., Brennan, J.D., Pelton, R.H. *J. Sol-Gel Sci Technol* **87** (2018) 657-664
- [6] Hong et al. *Optical Materials* **68** (2017) 11-18

Passive Filler Loaded Polysilazane-Derived Glass/Ceramic Coating Systems

I. Petříková¹, M. Parchovianský¹, P. Švančárek¹, G. Motz², D. Galusek¹

¹FunGlass - Centre for Functional and Surface Functionalized Glass, Department of Functional Materials, Študentská 2, 911 50 Trenčín, Slovakia
(E-mail: ivana.petrikova@tuni.sk)

²University of Bayreuth, Ceramic Materials Engineering, D-95440 Bayreuth, Germany

ABSTRACT

This study describes the development of a corrosion resistant environmental barrier coatings on AISI 441 stainless steel substrates. For that purpose, double layer polymer derived ceramic (PDC) coating systems consisting of a bond coat and a top coat were developed. In order to achieve well adherent coatings without failures, stainless steel substrates were cleaned by four different cleaning procedures, such as ultrasonic vibration cleaning in acetone, ethanol and deionised water, sandblasting with glass beads, chemical etching with Kroll's reagent and combination of these methods. The pre-treated substrates were then dip-coated in perhydropolysilazane (PHPS) solution to obtain bond coat. The pyrolysis of the bond-coat was performed in air at a temperature of 450 °C for 1 h. The subsequently applied top coat was prepared by mixing defined volume fractions of a liquid polysilazane HTT1800, ceramic filler particles (yttria-stabilized zirconia – YSZ, Al₂O₃-Y₂O₃-ZrO₂ powder - AYZ), and commercial glass frits (G018-281, Schott AG). The resulting mixture was applied by spray-coating technique. Parameters like the volume fraction of the HTT1800 polymer, filler and glass system were varied in order to optimise the coating systems. All coated samples were heat treated in air at 850°C for 1 h. The selected optimised compositions are listed in Tab.1.

Tab. 1: Compositions of the composite top coats before pyrolysis (vol. %)

	HTT1800	YSZ	G018-281	AYZ
D1	20	20	40	20
D2	25	20	35	20
D3	30	20	30	20

The surface morphology of pre-treated steel samples was examined by scanning electron microscopy (SEM) and roughness parameters were observed using atomic force microscope (AFM) and Raman spectroscopy. The results showed that chemical etching results in a surface with irregular morphology, while this treatment led to the slight roughening of the surface ($R_z = 0.88 \mu\text{m}$) compared to ultrasonically cleaned substrates ($R_z = 0.27 \mu\text{m}$). More uniform and compacted surface was achieved by the sandblasting with glass beads, while the average surface roughness R_z increased to a value of $1.70 \mu\text{m}$.

To investigate the bonding between the bond coat and steel substrate treated by different cleaning procedures, cross sections of the composition D2 were prepared for SEM examination (Fig.1). The chemical etching with the Kroll's reagent caused considerable changes in the microstructure and the chemistry of stainless steel and as a result, the bond coat peeled off the substrate. In the case of sandblasted samples, the sharp borders and peaks initiated the formation of cracks and spallation of bond coat in the coatings. On the other side, pre-treatment by ultrasonic cleaning in acetone, ethanol and deionised water was found to be the most effective. In order to clarify the bonding between the coating and steel, the selected coatings were tested under prolonged static exposure for 24 hours in air at 850 °C. After heat treatment, all coatings, except for those applied to ultrasonically cleaned substrates, delaminated or significant cracking was observed in

the bond coat.

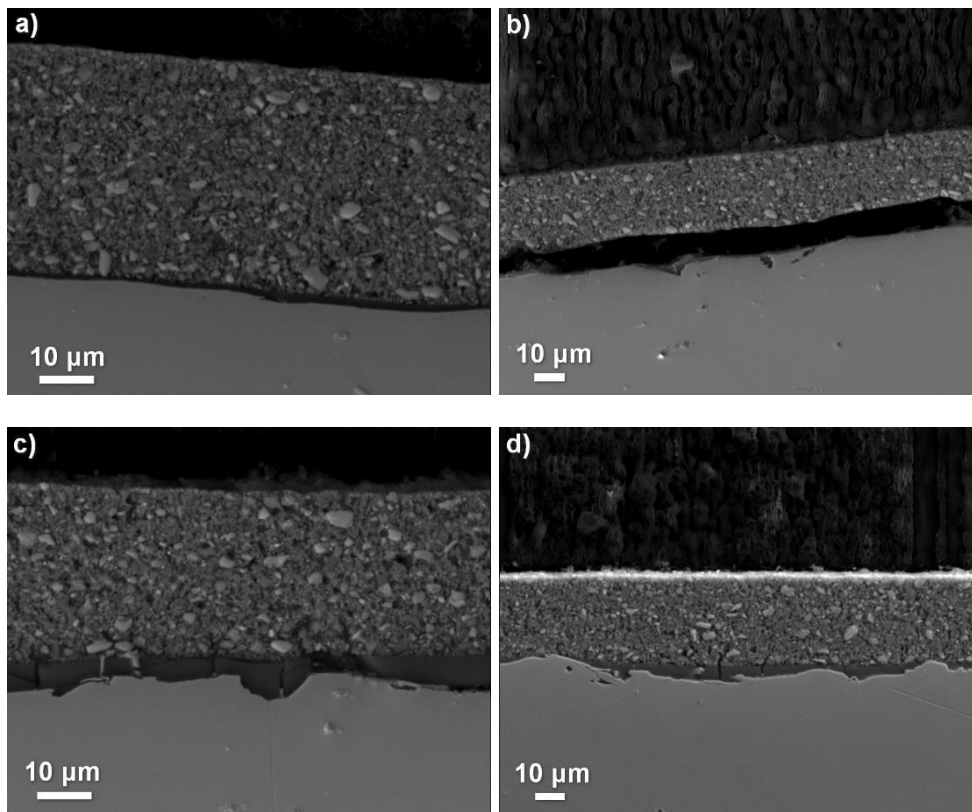


Fig. 1: SEM cross-sectional micrographs of the coating D2 applied to pre- treated steel substrates: a) ultrasonic cleaning, b) chemical etching, c) sandblasting, d) sandblasting + chemical etching

After a thermal treatment in air at 850 °C, the resultant coating applied to ultrasonically cleaned substrates with the thickness up to 40 μm is almost fully dense, with no cracking or delamination and it is expected to prevent the access of aggressive environment to the steel substrate at elevated temperatures. Additionally, this microstructure system with residual porosity is beneficial to the thermal stability of the coatings, as it contributes to the reduction of the thermal stresses during heating and cooling cycles. These results confirmed that the combination of PDC with tailored fillers and glass systems enable the processing of dense and crack free coating systems.

Keywords: bond coat, PDC coating, stainless steel

Acknowledgment:



This paper is a part of dissemination activities of project [FunGlass](#). This project has received funding from the European Union's Horizon 2020 research and innovation programme under grant agreement No 739566 and in the frame of the project Centre for Functional and Surface Functionalized Glass (CEGLASS), ITMS code is 313011R453, operational program Research and innovation, co-funded from European Regional Development Fund.

Passive filler loaded polysilazane-derived glass/ceramic coating system on AISI 441 stainless steel: Corrosion behaviour

M. Parchovianský¹, I. Petříková², P. Švančárek³, D. Galusek³, G. Motz⁴,

¹ Department of Coating Processes, FunGlass, Alexander Dubček University of Trenčín, Študentská 2, 911 50 Trenčín, Slovakia

(E-mail: milan.parchoviansky@tnuni.sk)

² Department of Functional Materials, FunGlass, Alexander Dubček University of Trenčín, Študentská 2, 911 50 Trenčín, Slovakia

³ Joint Glass Centre of the IIC SAS, TnUAD and FChFT STU, FunGlass, Študentská 2, 911 50 Trenčín, Slovakia

⁴ University of Bayreuth, Ceramic Materials Engineering, D-95440 Bayreuth, Germany

ABSTRACT

This study describes a corrosion resistant environmental barrier coating (EBC) applied to an AISI 441 stainless steel substrate. For that purpose, four polymer derived ceramic (PDC) coating systems consisting of a bond coat applied by dip coating and a top coat loaded with a passive filler deposited by spray coating are developed. The selected samples of PDC layers (C2-GM, C4-PP) are studied from the point of view of their corrosion resistance in the flow-through atmosphere of synthetic air at the temperatures up to 1000 °C. The ceramic coatings for corrosion tests were pyrolysed in the air for 1 hour at the temperature of 800 °C. The compositions selected for detailed corrosion tests are summarized in Tab. 2

Tab. 2: Compositions of the composite top coats after pyrolysis (vol. %) and estimated thermal expansion coefficients; (GM = glass microspheres, PP = precursor powder)

Sample name	HTT 1800	YSZ	G8470	G018-311	G018-385	AYZ	CTE (10 ⁻⁶ /K)
C2-GM	20	37	17	17	-	9 (GM)	8.9
C4-PP	20	30	-	13	16	21 (PP)	8.5

Weight increment of uncoated and coated samples as a function of the time at various temperatures are shown in Fig. 2a-c. At all three temperatures, the weight increases rapidly in the early stages, up to 6 hours. At 900 °C the weight gain slows down after 6 h of corrosion and it is eventually stabilized at times exceeding 12 h, indicating that a diffusion barrier of corrosion products was formed at the steel's surface. At 950 °C and 1000 °C the initial fast corrosion slows down significantly after 6 h, but continuous, and approximately linear mass increase is observed. For coated samples (Fig. 2b, c) weight gains at temperatures 900 °C and 950 °C were negligible in the whole tested time interval. Small weight loss observed in the C2-GM coating after 1 h test at 950 °C which was attributed to error in weight determination.

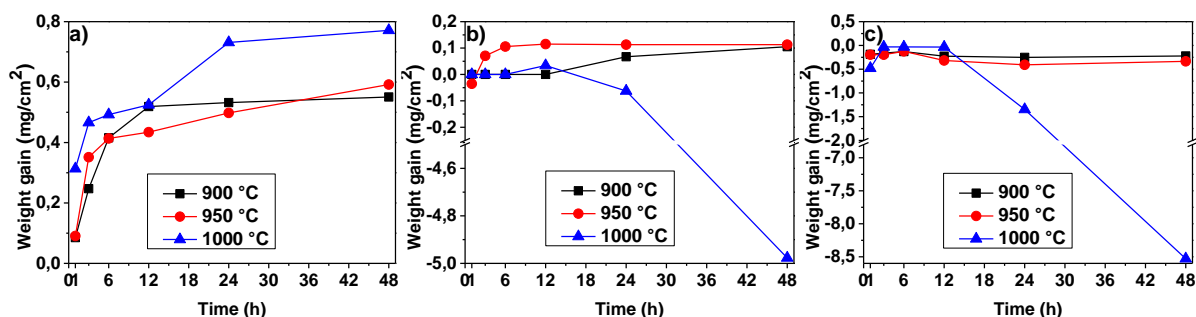


Fig. 2: Mass gain of steel and coatings after oxidation tests a) steel b) coat C2-GM, c) coat C4-PP

Time dependence of phase composition of corroded samples obtained by Rietveld refinement of X-ray diffraction data of uncoated steel and C2-GM, C4-PP coated steel substrates at temperature 950 °C are shown in Fig. 3 a-c. From the XRD patterns of steel substrates (Fig. 3a) the phases Fe, Cr₂O₃, TiO₂ and

spinel $(\text{Mn,Cr})_3\text{O}_4$ were identified. In the case of coated samples (Fig. 3 b,c), the dominant phases at all tested temperatures in the initial stages of oxidation (up to 6h) are monoclinic and tetragonal ZrO_2 . At longer exposure times and higher oxidation temperatures, crystallisation of the used glass fillers leads to the formation of new crystalline phases ($\text{Ba}(\text{AlSiO}_4)_2$ -hexacelsian, celsian), but also to the formation of new phases (YAG, $\text{YZr}_8\text{O}_{14}$) as a consequence of chemical reactions between the individual components of the layers. The product of substrate oxidation i.e. $(\text{Mn,Cr})_3\text{O}_4$ was observed after 24 hours of exposure of coated samples at 1000 °C.

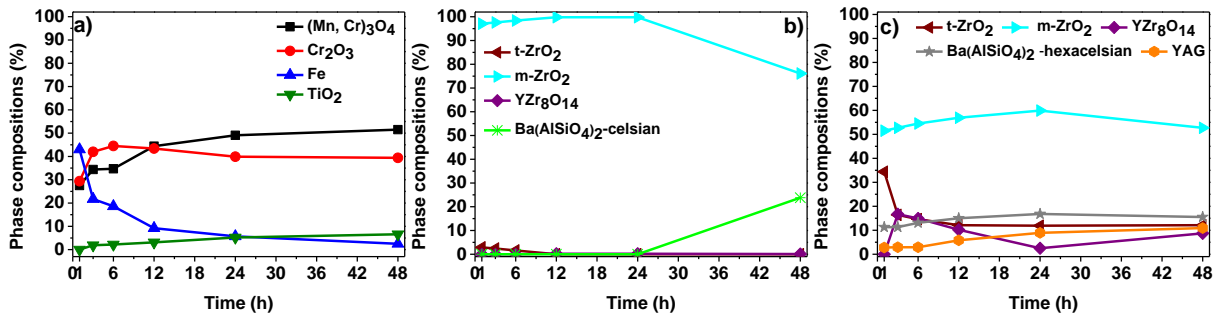


Fig. 3: Time dependence of phase composition of oxidized sample obtained by Rietveld refinement of X-ray diffraction data at the temperature 950 °C a) steel b) coat C2-GM, c) coat C4-PP

SEM micrographs of stainless steel and coatings after corrosion tests are shown in Fig. 4 a-c. The whole surface of uncoated steel is covered with a layer of oxide. In some cases, local delamination of the oxide layer (marked with the white arrows) was observed. After corrosion tests of coatings, there was a significant increase in the porosity of the layers and, accompanied by the growth of the pores and decrease of the coating thickness. Due to the softening of the used glass fillers, the cracks in the layers gradually healed, indicating at least partial protection of the metal substrate. A self-sealing process likely occurred during the test, allowing the protection of the stainless steel against further oxidation.

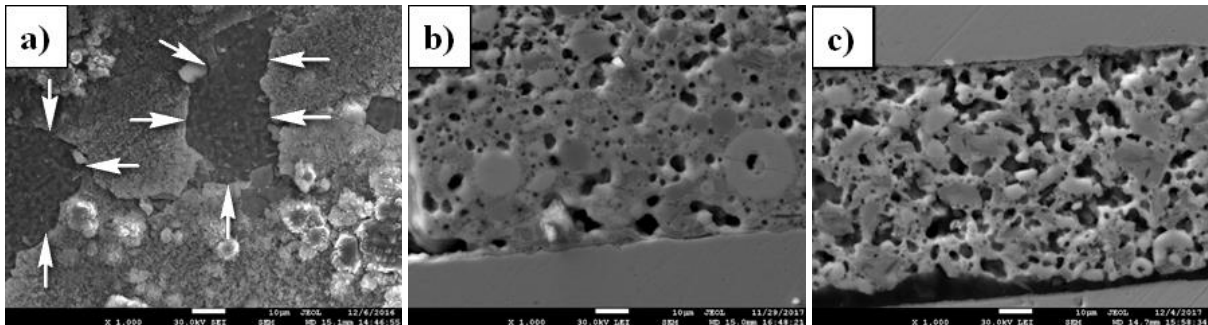


Fig. 4: Corrosion tests - microstructures a) steel 900°C/3h, b) C2-GM 950°C/6h, c) C4-PP 950°C/6h

Keywords: Corrosion, Passive filler, Polymer-derived ceramics

Acknowledgment:



This paper is a part of dissemination activities of project FunGlass. This project has received funding from the the grant APVV 0014-15 and the Deutsche Akademisch Austauschdienst (DAAD) grant scheme and European Union's Horizon 2020 research and innovation programme under grant agreement No 739566.

Effect of Corrosive Media on Hardness and Wear resistance of $\text{Li}_2\text{Si}_2\text{O}_5$ glass-ceramics

A. Švančárková^{1,2}, D. Galusková¹ and D. Galusek¹

¹ FunGlass, Centre for Functional and Surface Functionalized Glass, Department of Biomaterials, Alexander Dubček University of Trenčín, Študentská 2, 911 50 Trenčín, Slovakia
(E-mail: annasvancarkova@tnuni.sk)

²Faculty of Chemical and Food Technology STU, Radlinského 9, 812 37 Bratislava, Slovakia

ABSTRACT

The influence of corrosion in an acidic (4% acetic acid (pH=2.4)) and a basic media of NaOH (pH=10) on microhardness of lithium disilicate dental ceramics was studied. Three types of lithium disilicate glass ceramics were prepared by sintering of partially crystallized lithium metasilicate glass ceramics, with subsequent crystallization of lithium disilicate using two different two-stage heat treatment regimes: A - 500°C/2 h, + 850°C/2 h; B - 500°C/1 h + 820°C/1 h; and a one stage heat treatment C – 850 °C/1h. In all cases the heating and cooling rates were 5°C/min and 5°C/min, respectively. The temperatures were determined on the basis of data obtained from literature, where the first temperature was applied to nucleate lithium disilicate, while the second temperature was used to grow the lithium disilicate crystals. This way the materials with various mechanical properties and corrosion resistance were prepared.

The influence of corrosion in acidic and basic media on properties of dental glass ceramics was monitored on the basis of results of the tests carried out both under quasi-dynamic and static conditions. The quasi-dynamic test was performed at the temperature corresponding to the temperature of human body (37°C). In both media, the samples were corroded for 96 h with exchange of the corrosion medium for a fresh one in 12 h intervals. Under static conditions the samples were tested at 80°C for 16 h without a change of the corrosion medium of 4% acetic acid (ISO 6872, Standards for hydrolytic resistance of dental ceramics materials).

The microhardness was determined by Vickers indentation at the load of 1.0 N on mechanically polished surfaces of dental ceramics before and after corrosion. The microhardness of materials A and B was identical (for A: 625±4 HV1.0, for B: 625±8 HV1.0). For the material C slightly lower value was measured (607±10 HV1.0). After static corrosion test in 4% acetic acid the Vickers hardness of material A decreased from 625±4 HV1.0 to 594±4 HV1.0. After dynamic test in the same corrosion medium the decrease was less pronounced, to 605±8 HV1.0. Dynamic corrosion test in basic solution with pH 10 led to decrease of microhardness to 599±13 HV1.0. The corrosion in basic or acidic solutions had no significant impact on microhardness of materials B and C. The contents of the elements leached into the solution of corrosion media during corrosion were determined by atomic emission spectrometry (AES) with inductively coupled plasma. The major elements leached from dental ceramics were lithium, phosphorus and potassium in the acidic environment, and phosphorus, lithium and silicon in basic solutions. Highest resistance against corrosion acid environment was measured for the material B. Corrosion resistance in alkaline medium was similar for all materials. Wear resistance of both corroded and un-corroded materials was tested by tribometry measurements in dry conditions using ball-on-flat technique. The tribological partner was a highly polished alumina ball 6.35 mm in diameter, the applied load was 10 N, sliding speed 10 cm/s and sliding distance was 50 m. Wear of uncorroded materials A and B was the same ($5.8 \times 10^{-4} \pm 4 \times 10^{-5} \text{ mm}^3/\text{Nm}$), wear of the un-corroded material C was slightly lower ($5.5 \times 10^{-4} \pm 5 \times 10^{-5} \text{ mm}^3/\text{Nm}$). The corrosion both in basic or acidic environment under dynamic conditions caused a decrease in wear resistance of all tested samples. Wear of material A was after corrosion in basic environment $6.0 \times 10^{-4} \pm 3 \times 10^{-5} \text{ mm}^3/\text{Nm}$, in acidic environment $6.8 \times 10^{-4} \pm 4 \times 10^{-5}$. Wear of material B increased after corrosion in basic solution to $5.8 \times 10^{-4} \pm 8 \times 10^{-5}$, after corrosion in 4% acetic acid to $6.4 \times 10^{-4} \pm 6 \times 10^{-5}$. Wear of C increased from $5.5 \times 10^{-4} \pm 5 \times 10^{-5} \text{ mm}^3/\text{Nm}$ to $6.5 \times 10^{-4} \pm 6 \times 10^{-5} \text{ mm}^3/\text{Nm}$ after corrosion in acidic medium and to $6.3 \times 10^{-4} \pm 10 \times 10^{-6} \text{ mm}^3/\text{Nm}$ in NaOH solution.

However, the corrosion test according to the ISO 6872 led to an increase in wear resistance. Wear decreased from $5.8 \times 10^{-4} \pm 4 \times 10^{-5}$ to $5.4 \times 10^{-4} \pm 2 \times 10^{-5}$ mm³/Nm for material A, from $5.8 \times 10^{-4} \pm 4 \times 10^{-5}$ to $5.4 \times 10^{-4} \pm 4 \times 10^{-5}$ mm³/Nm for B and from $5.5 \times 10^{-4} \pm 5 \times 10^{-5}$ to $4.5 \times 10^{-4} \pm 4 \times 10^{-5}$ mm³/Nm for C material. The decrease could cause the formation of a lubrication layer of the non-analyzed composition. After extended contact with acidic or basic solutions all studied ceramic materials displayed evidence of surface structural changes, as confirmed by examination of corroded surfaces by scanning electron microscopy. Degradation of micromechanical properties, i.e. decrease of wear resistance (dynamic corrosion conditions) and of Vickers microhardness (material A) was confirmed.

Keywords: lithium disilicate dental ceramics, corrosion, microhardness, wear resistance

Acknowledgment:



This paper is a part of dissemination activities of project [FunGlass](#).
This project has received funding from the European Union's Horizon 2020 research and innovation programme under grant agreement No 739566.

Corrosion of IZOMER TT Glass Fiber Under Static Conditions In Distilled Water And In Borate Coolant Solution

Jana Vokelová Vráblová¹, Jaroslava Micháľková¹, Mária Chromčíková^{2,3}, Branislav Hruška⁴, Marek Liška^{2,3}

¹FunGlass, A. Dubcek University of Trenčín, Študentská 2, SK-911 50 Trenčín, Slovakia

²VILA – Joined Glass Centre of the IIC SAS, TnUAD, FChPT STU, Študentská 2, SK-911 50 Trenčín, Slovakia

³VILA, FunGlass, A. Dubcek University of Trenčín, Študentská 2, SK-911 50 Trenčín, Slovakia

⁴Central Laboratories, FunGlass, Alexander Dubček University of Trenčín, Študentská 2, SK-911 50 Trenčín, Slovakia

ABSTRACT

Large amounts of glass fibers are used as thermal insulation in nuclear power plants (NPPs). In the event of a loss of coolant accident (LOCA) [1–4] the insulation is mechanically destroyed by steam impact and drops to the bottom of the reactor containment, where it is immersed in the alkaline coolant liquid. According to alkali resistance of the commercially produced thermal fibrous insulations glass dissolution occurs, followed by later re-precipitation from the over-saturated solutions. A fraction of the fibers is also captured on the sump screen and thus prevents recirculation of the coolant in the emergency cooling system. Since the partially dissolved fibers can be mechanically destroyed (crushed), they can block the strainer causing failure of the emergency cooling system. In this situation the high head loss reaches a value that disables the operation of the pumps. The above effect of strainer blocking can be dramatically enhanced by strengthening of the fiber bed by the re-precipitated matter. Therefore study of the kinetics and thermodynamics of glass dissolution is needed for correct modeling of the process and its consequences on the operability of the emergency systems [5]. Chemical durability of glass with the composition of glass fibrous insulation IZOMER TT commonly used in nuclear power plants reactor containment was tested by static leaching tests at 70°C, 80°C, and 90°C. Distilled water and borate coolant solution were used as corrosive media. The semiempirical kinetic model based on the Aagaard Helgeson kinetic equation was proposed and qualified. Proposed model enables prediction of glass dissolution kinetics for various time–temperature schedules proposed for different Loss of Coolant Accident scenarios.

Keywords: Glass corrosion, LOCA, Glass fiber insulation, Coolant solution, Glass grain, Kinetics.

Acknowledgment:



This paper is a part of dissemination activities of project [FunGlass](#). This project has received funding from the European Union's Horizon 2020 research and innovation programme under grant agreement No 739566. This work was supported by The Slovak Grant Agency for Science under grant No. VEGA 2/0088/16, VEGA

1/0064/18.

References:

1. Zigler G., Beaty R., Brideau J., Comes L., Rao D.V., Ruiz N., Sciacca F., Sharrer C., Thomas W., Walsh R. (1994): Parametric study of the potential for BWR ECCS strainer blockage due to LOCA generated debris. *NUREG/CR-6224 SEA No. 93-554-06-A:1*,
2. Rao D.V., Shaffer C.J., Leonard M.T., Ross K.W.(2003): Knowledge base for the effect of debris on PWR ECCS performance. *NUREG/CR-6808 LA-UR-03-0880*.
3. Park J.H., Kasza K., Fisher B., Oras J., Natesan K., Shack W.J.(2006): Chemical Effects Head – Loss Research in Support of Generic Safety. *NUREG/CR-6913 ANL-06/41*, Issue 191.
4. Soltész V., Vicena I., Liška M., Galusková D., Mattei J.M. (2012): Corrosion of Bourre glass fibers in borate water solution. *Glass Technol.: Eur. J. Glass Sci. Technol. A*, 53, 139–145 .
5. Soltesz V., Vicena I., Chromčíková M., Liška M., Mattei J.M. (2008): Chemical durability of glass thermal insulation fibers in borate and phosphate water solutions. *Adv. Materials Research* 39-40, 363-366.

Corrosion of 3Y-TZP ceramics for dental applications

A. Nowicka¹, H.F. El-Maghraby², D. Galusková¹ and D. Galusek¹

¹Centre for functional and surface functionalized glass, Alexander Dubček University of Trenčín, Slovak Republic

(E-mail: aleksandra.nowicka@tnuni.sk)

² Joint Glass Centre of the IIC SAS, TnUAD, FChPT STU, FunGlass, Alexander Dubček University of Trenčín, Trenčín, Slovakia

ABSTRACT

Due to its excellent properties 3Y-TZP ceramic is a suitable material for various applications, including dental materials for implants or crowns. One of the advantages of this material is its non-metallic nature, which is important for patients allergic to metals, including titanium [1]. However, the long-term surface stability of this material in a humid environment is still a matter of concern and may limit its application [2]. Additionally, the oral environment is very diverse and the surface of dental materials is exposed to different pH ranges, which could be highly acidic because of consumption of food and beverages, and conditions associated with reflux of gastric fluid [3]. Apart from the change of pH, substantial temperature fluctuations occur in the oral cavity.

The aim of this work was to study the long-term corrosion behavior of commercial and non-commercial 3Y-TZP ceramics in acidic environment and the influence of the loss of ions stabilizing tetragonal zirconia on tetragonal-to-monoclinic phase transformation of zirconia. This work also attempts to answer the question whether acid-related corrosion is a process, which is, by its nature and mechanism, different from low-temperature degradation (LTD). In addition, the influence of the loss of tetragonal zirconia stabilizing ions (Y^{3+}) on sensitivity of studied materials to LTD was also studied.

Two commercial materials were tested: zirconia-based dental materials stabilized in their tetragonal form by addition of yttrium (3Y-TZP) – IVOCLAR IPS e.max[®] ZirCAD and DOCERAM Nacera[®]. In addition, non-commercial 3Y-TZP ceramics have been prepared from a zirconia powder stabilized by the addition of 3 mol% of yttria and synthesized by hydrothermal process. Green bodies prepared by axial pressing of granulated powder at 50 MPa in a steel die were sintered for 2 h at 1450°C (3Y-TZP-1450) or 1500°C (3Y-TZP-1500). Sintered and polished ceramics have been corroded in 4% acetic acid at three different temperatures (37°C, 60°C, 80°C) with maximum duration of the test: 31 days (IVOCLAR and DOCERAM) and 40 days (ceramics prepared in our laboratory). For DOCERAM and IVOCLAR the corrosion tests at 37°C and 60°C were extended, respectively up to 265 days and 130 days. The kinetics of LTD was evaluated by performing the Accelerating Aging Test (AAT) in water steam at 134°C, under the pressure of 2 bars. It has been postulated [4], that 1 h in an autoclave under these conditions roughly corresponds to 1-4 years in-vivo at 37°C. Corrosion and aging effects, expressed in terms of the amount of monoclinic zirconia formed at the material's surface as the result of phase transformation of tetragonal zirconia, were monitored with the use of the X-ray powder diffractometer Panalytical Empyrean with Bragg-Brentano geometry at a range of $2\theta = 10^\circ - 80^\circ$ using $CuK\alpha$ radiation with a wavelength of 0.15405 nm. To monitor the amount of leached ions from the materials during the corrosion tests chemical analysis of corrosion media was carried out using the mass spectrometry in inductively coupled plasma (ICP – MS, Agilent 7900).

Acidic corrosion of 3Y-TZP dental ceramics was associated with leaching of stabilizing ions from zirconia ceramics. Depletion of yttrium ions increased with temperature (Table 1.). In the case of 3Y-TZP-1450, the highest observed amount of leached yttrium represents almost 30% of all the content of yttrium in this material. Measurable phase transformation was observed already after 40 days at 37°C: no monoclinic zirconia was detected under these conditions in other tested materials. Significant increase of the monoclinic phase content in DOCERAM, IVOCLAR and 3Y-TZP-1500 was observed only after exposure of the materials to corrosive medium at 80°C. The least corrosion resistant commercial and non-commercial materials, i.e. IVOCLAR and 3Y-TZP-1450 were tested also in

deionized water, as a reference medium. While the transformation rate was similar to that obtained during the corrosion in 4% acetic acid, the acidic environment accelerated depletion of yttrium ions to the solution and was more aggressive than deionized water (Table 1).

The kinetics of tetragonal to monoclinic phase transformation was described by the Mehl-Avhrami-Johnson (JAM) equation [5]. Calculated activation energies of tetragonal to monoclinic phase transformation for IVOCLAR, 3Y-TZP-1450 and 3Y-TZP-1500 were respectively calculated as follows: 78.72 ± 0.01 kJ/mol, 65.00 ± 6.06 kJ/mol and 92.60 ± 18.38 kJ/mol. Fig. 1 shows the time dependencies of experimental (from corrosion tests in acetic acid) and calculated monoclinic phase contents at various temperatures ranging from 37°C to 134°C, respectively for 3Y-TZP-1450 (Fig. 1. a)) 3Y-TZP-1500 (Fig.1 b)) and IVOCLAR (Fig.1 c)). The actual content of the monoclinic phase in the initial stages of the experiment was in all cases slightly lower than the calculated ones. However, at longer exposure to corrosive media, the measured and calculated data overlap. The expected time to transform to more than 80% of monoclinic phase in the tested materials at 37°C can be then estimated as follows: IVOCLAR: 7 years, 3Y-TZP-1450: 1 year, 3Y-TZP-1500: 18 years. However, the transformation of the 3Y-TZP-1500 could be overestimated, due to the high standard deviation of the activation energy. For DOCERAM, no kinetics for lower temperatures were measured and the predicted transformation could not be calculated. The collected data from this study indicated that there was no significant impact of depletion of the stabilizing yttrium ions on phase transformation in tested commercial materials and the material 3Y-TZP-1500 prepared in our laboratory. The transformation, which occurs after corrosion at temperatures higher than 37°C, was correlated with nucleation and growth processes. The calculated activation energies are comparable to those obtained by other authors [6], [7].

Table 1. Normalized amount of yttrium ions leached out from tested materials in different aqueous solutions; duration of the experiment for commercial materials was 31 days and for non-commercial materials, 40 days.

Temperature of the experiment	IVOCLAR		DOCERAM	3Y-TZP-1450		3Y-TZP-1500
	4% acetic acid $\mu\text{g}/\text{cm}^2$	Water $\mu\text{g}/\text{cm}^2$	4% acetic acid $\mu\text{g}/\text{cm}^2$	4% acetic acid mg/cm^2	Water $\mu\text{g}/\text{cm}^2$	4% acetic acid $\mu\text{g}/\text{cm}^2$
37°C	4.2 ± 0.7	-	1.3 ± 0.5	0.16 ± 0.19	-	8.9 ± 2.1
60°C	6.9 ± 0.4	-	2.2 ± 0.5	0.57 ± 0.1	-	7.9 ± 0.9
80°C	8.7 ± 0.1	3.8 ± 1.5	3.2 ± 1.5	9.9 ± 0.2	92.4 ± 14.7	24.8 ± 0.7

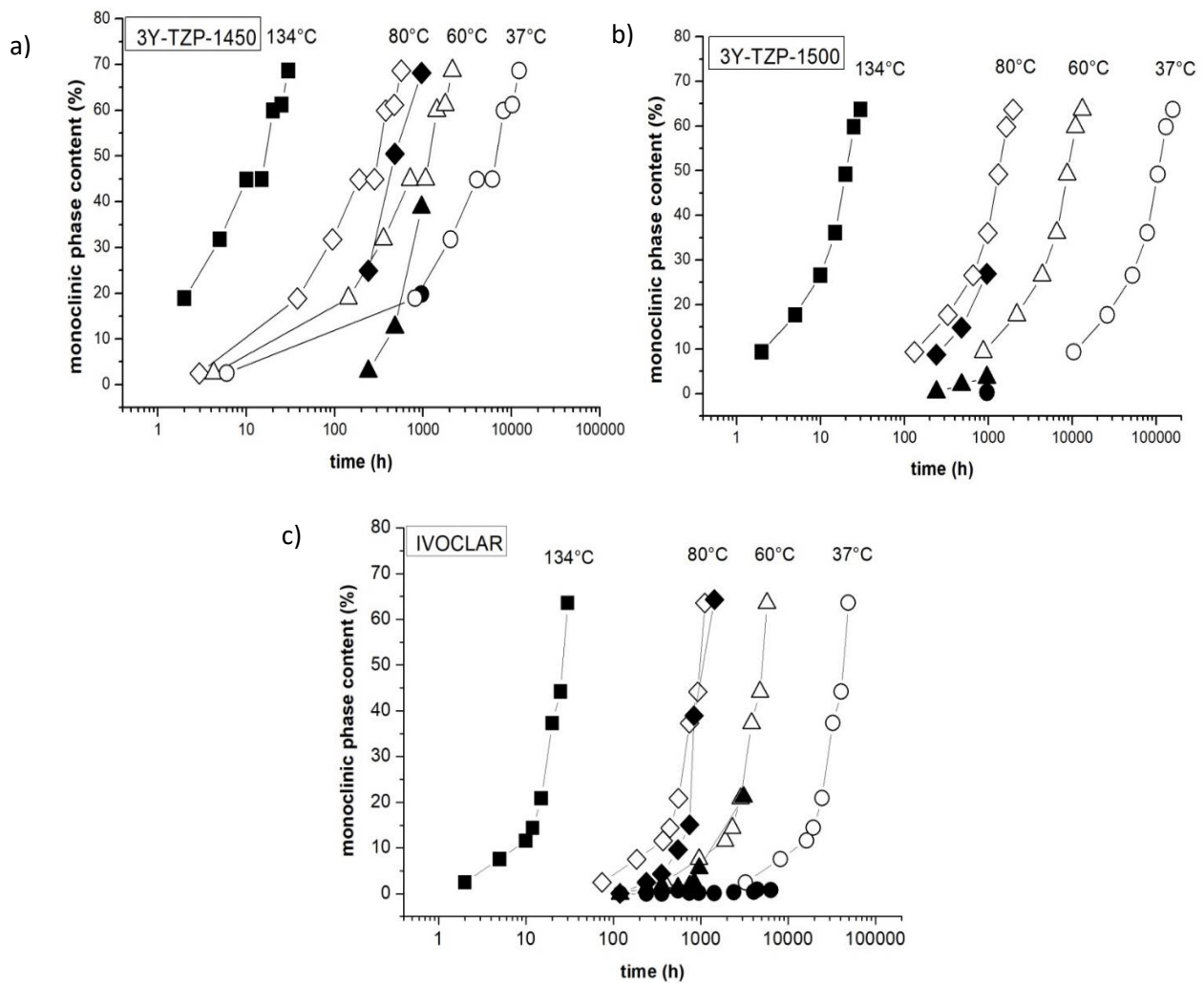


Fig. 1. Relationship between the amount of monoclinic phase and aging time at various temperatures: comparison of measured data with the values estimated from the MAJ equation: solid dots represent experimental data, empty dots are the values calculated from the MAJ equation: a) 3Y-TZP-1450, b) 3Y-TZP-1500, c) IVOCLAR

Keywords: acetic acid, Accelerated Aging Tests, corrosion, dental ceramics, LTD, Y-TZP. ;

Acknowledgment:



This paper is a part of dissemination activities of project [FunGlass](#). This project has received funding from the European Union's Horizon 2020 Research and innovation program under grant agreement No 739566. The financial support of this work by the grant APVV 0014-15 is gratefully acknowledged.

References:

- [1] C. Sanon, J Chevalier, T. Douillard, M. Cattani-Lorente, S.S. Scherrer , L. Gremillard, "A new testing protocol for zirconia dental implants," *Dental Materials* 31, pp. 15-25, 2015.
- [2] J. Cotic, P. Jevnikar, A. Kocjan, , "Ageing kinetics and strength of airborne-particle abraded 3Y-TZP ceramics," *Dental Materials* 33, pp. 847-856, 2017.
- [3] M. V. Swain, "Impact of oral fluids on dental ceramics: What is the clinical relevance?," *Dental Materials* 30, pp. 33-42, 2014.
- [4] T. Douillard, J. Chevalier, A. Descamps-Mandine, I. Warner, Y. Galais, P. Whitaker, J.J. Wu,

Q.Q. Wang, "Comparative ageing behaviour of commercial, unworn and worn 3Y-TZP and zirconia toughened alumina hip-joints heads," *Journal of the European Ceramic Society* 32, pp. 1529-1540, 2012.

- [5] J. Chevalier, L. Gremillard, S. Deville, "Low-Temperature Degradation of Zirconia and Implications for Biomedical Implants," " *Annual Review of Materials Research*, pp. 1-32, 2007.
- [6] Ch. Wei, L. Gremillard, "Toward the prediction of hydrothermal ageing of 3Y-TZP bioceramics from processing parameters," *Acta Materialia*, pp. 245-256, 2018.
- [7] V. Luggi, V. Sergo, "Low temperature degradation - aging- of zirconia: A critical review of the relevant aspects in dentistry," *Dental Materials* 26, pp. 807-820, 2010.

Crystallisation of TiO₂ Xerogel

Plško A.¹, Pagáčová J.², Papučová I.², Prnová A.¹, Valúchová J.¹, Hruška B.¹

^{1*} FunGlass – Centre for Functional and Surface Functionalized Glass, Alexander Dubček University of Trenčín, Študentská 2, 911 50 Trenčín, Slovakia
(*E-mail: alfonz.plsko@tnuni.sk)

² Faculty of Industrial Technologies in Púchov, Alexander Dubček University of Trenčín

ABSTRACT

Nanomaterials based on titanium dioxide has a wide usage, mainly in the form of films in the solar systems and environmental applications. In these films, TiO₂ is required to be in the form of anatase. This crystalline form is formed in the films during their thermal treatment. Sol-gel method represents advantageous method for preparation of TiO₂ films. In this method, the controlled reactions of hydrolysis and condensation of titanium isopropoxide lead to preparation of TiO₂ sol which is transformed to gel and subsequently to xerogel after the sol is deposited on the substrate. Mentioned transformation is carried out by drying up to the temperatures of 100 °C. The subsequent thermal treatment at temperatures around the 400 °C causes the transformation of xerogel to anatase. For achievement of the best properties of prepared films, the process of thermal treatment has to be controlled. For optimizing of thermal treatment process, it is needed to understand and observe which processes take place during the transformation from xerogel to crystalline form – anatase.

Processes which take place during the thermal treatment of xerogel were observed using DTA/TG analysis at heating rates of 10 and 2 °C/min. On the basis of analysis of DTA/TG curves, the individual processes during the thermal treatment have been identified. It was found, that in the range of temperatures, where the crystallization of anatase is assumed, there are also the processes which are connected with weight loss. Based on the mentioned fact, the process of thermal treatment of TiO₂ xerogel was observed using high-temperature Raman spectroscopy and high-temperature X-ray diffraction. In relation to the formation of anatase, the intervals of temperatures were identified. Based on the comparison of results of all analyses, it can be concluded that the anatase is formed from xerogel by the given reactions – the first reaction represents the decomposition of xerogel leading to the formation of amorphous TiO₂ and the second reaction represents the formation of anatase, respectively.

Keywords: Titania xerogel, Crystalization, Sol-gel, DTA/TG, Raman spectroscopy, HTXRD

Acknowledgment: The research was supported by the projects VEGA 1/0589/17 and VEGA 1/0431/18.



This paper is a part of dissemination activities of project [FunGlass](#).
This project has received funding from the European Union's Horizon 2020 research and innovation programme under grant agreement No 739566.

Solid-state fabrication of transparent YAG ceramics for optical applications: Characterization mixing, and processing of the starting oxides

**H.F. El-Maghraby^{1,2,3}, J. Sedláček⁴, P. Švančárek^{1,2}, M. Kachlík⁵, T. Spusta⁵, K. Maca⁵,
D. Galusek^{1,2}**

¹ Joint Glass Centre of the IIC SAS, TnUAD and FChPT STU, Trencin, Slovakia

² Centre for Functional and Surface Functionalized Glass, Alexander Dubcek University of Trencin, Slovakia

³ Ceramics Dept., National Research Centre, NRC, El-Bohouth St., Dokki, Giza, 12622 Egypt

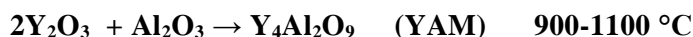
⁴ Institute of Inorganic Chemistry, SAS, Dúbravská cesta 9, 84536 Bratislava, Slovakia

⁵ CEITEC BUT, Brno University of Technology, Technická 10, Brno 616 00, Czech Republic

(Corresponding author: hesham.abdelrehim@tuni.sk)

Polycrystalline yttrium aluminum garnet ceramic laser material ($Y_3Al_5O_{12}$) or YAG is one of the most common candidates that received much attention since 1995 due to its optical characteristics that has been improved greatly and its highly efficient laser oscillation that could be obtained [1]. Moreover, in the case of laser applications, some recent works demonstrated the rare-earth-doped YAG ceramics to be even better than the single crystals [2,3].

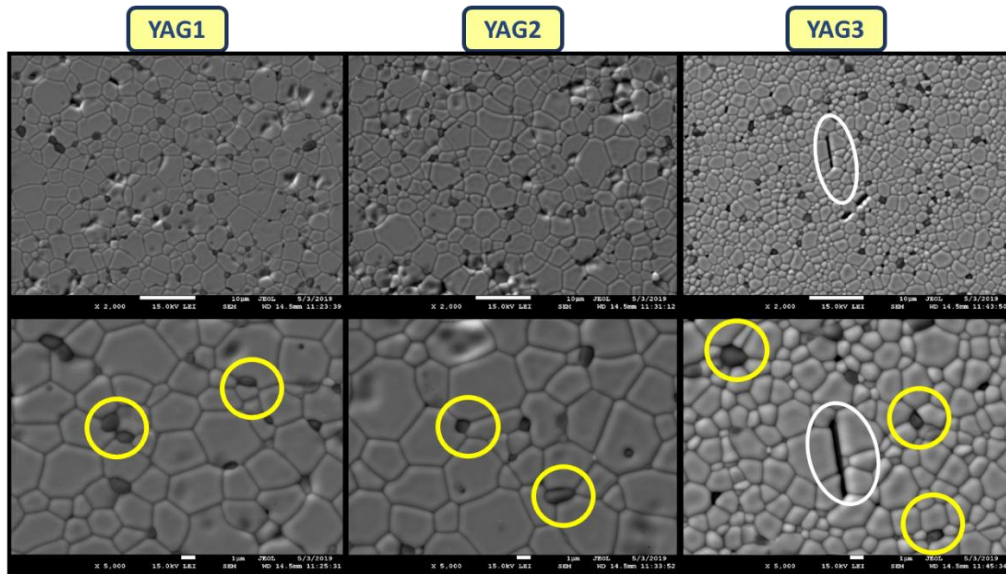
For the last thirty years, massive attention has been focused on the performance of YAG ceramics fabrication methods [4-7]. Compared with the complicated wet-chemical techniques of YAG nanopowders synthesis [8,9] the solid-state reactive sintering is considered as the easiest and cost efficient way for achieving of YAG desired properties. In this way, commercial high purity α - Al_2O_3 and Y_2O_3 powders are mixed in precise stoichiometric quantities where the required YAG phase formation occurs during the sintering step. It has been proved that the Al_2O_3 - Y_2O_3 system experienced three different crystallographic phases during the sintering. The phase composition and formation temperature ranges for each phase are described as follows [10]:



So, great attention has to be paid during the sintering reaction to avoid the presence of any secondary YAP or YAM phases which interfere with the YAG cubic structure and inhibit the propagation of light through the material thus strongly deteriorating the optical properties. Moreover, the most important issue in the transparent YAG ceramics is the removal of pores, which is achieved through the use of sintering additive and application of vacuum or pressure during sintering. Although tetraethyl orthosilicate (TEOS) and MgO served as a common sintering additive for the densification promotion [11,12], the priority was given to the use of MgO where a successful fabrication of YAG transparent ceramic with excellent optical properties was achieved by employing a simple solid state reaction vacuum sintering using 0.03 wt. % MgO. The transmittance was 84.5% at 1064 nm, after sintering the sample at 1820°C for 8 h [12].

In the present study, commercial high purity α - Al_2O_3 and Y_2O_3 powders were mixed in precise stoichiometric quantities where the required YAG phase formation occurs during the sintering step. In addition, a small amount (0.03 wt.%) MgO or the equivalent amount of $Mg(NO_3)_2 \cdot 6H_2O$ was used both as a sintering aid and grain growth inhibitor. The mixed oxide suspensions were subjected to freeze granulation and freeze drying before uniaxial pressing at 30 MPa for 30 sec then cold isostatic pressing at 300 MPa for 5 min. Characterization of the starting oxide mixtures prepared by using of different methods, mixing conditions, and processing steps was carried out with the aim to achieve the optimum green body characteristics prior to the sintering process. Results revealed that both the phase composition and microstructure of the obtained YAG ceramics are noticeably affected by the factors such as morphology and particle size of the starting powders. Moreover, the impact of pore size distribution, different shaping parameters, density of the green body,

densification behavior of samples pre-sintered at 1675°C for 4h in air and those furtherly hot isostatically pressed at 1700°C for 4h and 200 MPa in argon atmosphere results were elucidated.



SEM of different YAG samples, YAG1 is sintering aid free, YAG2 is with 0.03 wt% of MgO, and YAG3 is with $\text{Mg}(\text{NO}_3)_2 \cdot 6\text{H}_2\text{O}$ equivalent to 0.03 wt% of MgO.

Keywords: Hot isostatic pressing, Solid-state reaction, YAG transparent ceramics.

Acknowledgment:



This paper is a part of dissemination activities of project [FunGlass](#).

This project has received funding from the European Union's Horizon 2020 research and innovation programme under grant agreement No 739566. This work is also financially supported by the grants VEGA 2/0026/17 and SAS-MOST 2015/06.

References:

1. A. Ikesue, et al., Fabrication and optical properties of high-performance polycrystalline Nd:YAG ceramics for solid-state lasers, *J. Am. Ceram. Soc.* 78 (4) (1995) 1033-1040.
2. J. Li, et al., Solid-state reactive sintering and optical characteristics of transparent Er:YAG laser ceramics, *J. Am. Ceram. Soc.* 95 (2012) 1029-1032.
3. F. Tang, et al., High efficient Nd:YAG laser ceramics fabricated by dry pressing and tape casting, *J. Alloys Compd.* 617 (2014) 845-849.
4. M. L. Saladino, et al., Synthesis of Nd:YAG nanopowder using the citrate method with microwave irradiation, *J. Alloys Compd.* 491 (2010) 737-741.
5. J. S. Li, et al., A novel stearate melting method for synthesizing highly reactive YAG nanopowders, *J. Alloys Compd.* 585 (2014) 48-53.
6. L. Zhang, et al., Systematic optimization of spray drying for YAG transparent, *J. Eur. Ceram. Soc.* 35 (2015) 2391-2401.
7. G. F. Fan, et al., Reduce synthesis temperature and improve dispersion of YAG nanopowders based on the co-crystallization method, *J. Alloys Compd.* 618 (2015) 1-6.
8. X. Li, et al., Synthesis of Nd³⁺ doped nanocrystalline yttrium aluminum garnet (YAG) powders leading to transparent ceramic, *Opt. Mater.* 29 (2007) 528-531.
9. J. S. Li, et al., A homogeneous co-precipitation method to synthesize highly sinterability YAG powders for transparent ceramics, *Ceram. Int.* 41 (2015) 3283-3287.
10. S. H. Lee, et al., Solid-state reactive sintering of transparent polycrystalline Nd:YAG, *J. Am. Ceram. Soc.* 89 (2006) 1945-1950.
11. R. Yin, et al., Fabrication of Nd:YAG transparent ceramics by non-aqueous gelcasting and vacuum sintering, *J. Eur. Ceram. Soc.* 36 (2016) 2543-2548.
12. T. Zhou, et al., MgO assisted densification of highly transparent YAG ceramics and their microstructural evolution, *J. Eur. Ceram. Soc.* 38 (2018) 687-693.

White light emitting Y₂O₃ based fluorescents doped by ZnO

P. Švančárek¹, R. Klement², W. Wisniewski³ and D. Galusek¹

¹ Dpt. VILA – Joint Glass Centre of the IIC SAS, TnUAD, FChPT STU, Študentská 2, 911 50 Trenčín, Slovakia
FunGlass, A. Dubček University of Trenčín, Študentská 2, 911 50 Trenčín, Slovakia

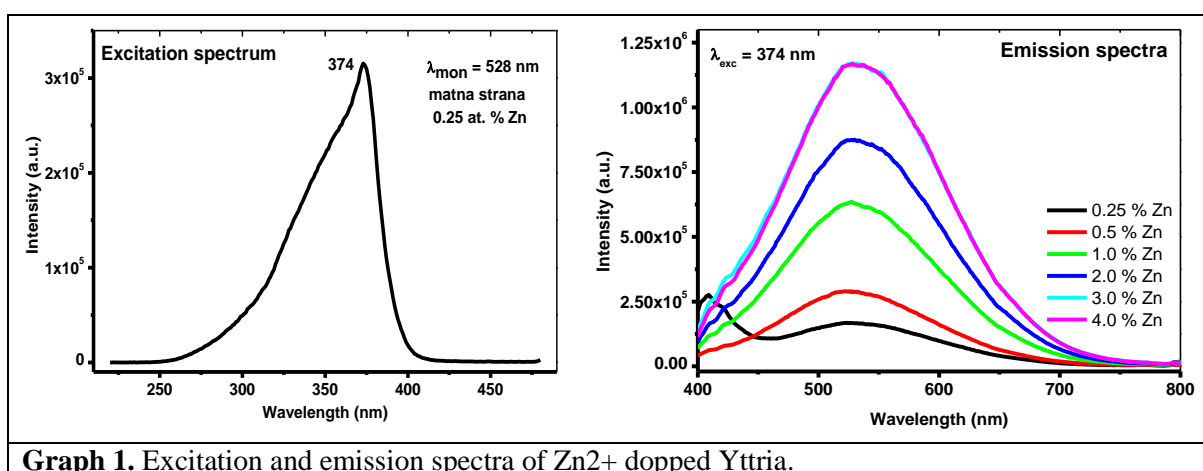
² Dept. of Functional Materials, FunGlass, Alexander Dubček University of Trenčín, Študentská 2, 911 50
Trenčín, Slovakia

³ Centre for Functional and Surface Functionalized Glass, Alexander Dubček University of Trenčín, 911 50
Trenčín, Slovakia

ABSTRACT

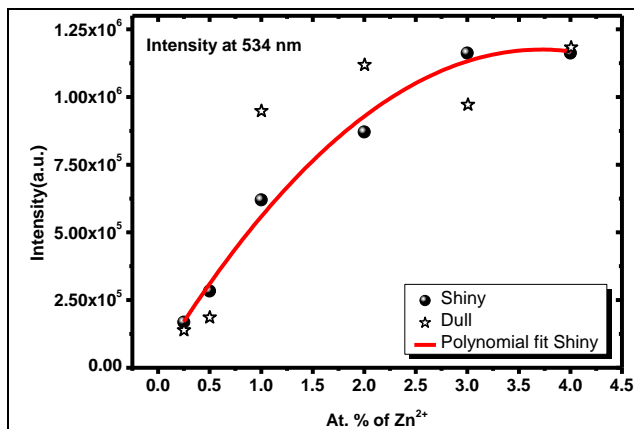
In this work we investigated fluorescence activity of yttria ceramic materials modified by various amounts of ZnO. Samples were prepared by pressure filtration of isopropanol based suspension containing 5 vol% of yttria, stabilized by 1 wt.% of PEG (Polyethylene Glycol 400 Ultra f. Fluka) in consideration of Y₂O₃ mass. After drying, the green pellets were presintered with regime: ramp 10°C/min to 1000°C and 1hour holding time followed by free cooling as to obtain porous but sufficiently stable pellets able to withstand infiltration procedure in water based solution. Water solutions of zinc acetate (Zn(CH₃COO)₂ · 2H₂O p.a. f. CentralChem) was used for infiltration with concentrations calculated individually accordingly to porosity of presintered pellets to obtain 0.25, 0.5, 1.0, 2.0, 3.0, 3.5 and 4 atomic percent of Zn²⁺ dopant. The pellets were sintered using superkantal furnace f. Netzch by following regime: ramp 10°C/min to 80°C and 2 hours holding time, ramp 10°C/min to 250°C and 2 hours holding time and finally, ramp 10°C/min to 1400°C and 2hour holding time followed by free cooling. To confirm the role of vacancies on fluorescence intensities, for the sample composition with strongest fluorescence activity the final sintering step temperature was changed to 1300°C and 1500°C with holding times 2h.

After sintering, both emission (PL) and excitation (PLE) fluorescence spectra were measured by Fluorolog 3 (FL3-21, Horiba) fluorescence spectrometer in front-face mode. The Xe-lamp (450 W) was used as an excitation source. All emission spectra, were corrected for spectrometer optics and excitation lamp response. Excitation spectra (PLE) spectra were corrected for the spectrometer response (optics). All spectra were recorded at the same conditions (slit width, integration time, monitored wavelength, filter) On graph 1. we can see stacked spectrums of prepared specimens. The strongest intensities were observed for 3 and 4 atomic at. % of Zn²⁺.



Graph 1. Excitation and emission spectra of Zn²⁺ doped Yttria.

For further evaluation the graph 2. was prepared to show photoluminescence intensities for different samples dopant concentrations at emission wavelength of 534nm. Using this graph, we can predict that the maximum intensity of luminescence for yttria doped ceramic will be around 3.5 at. % of Zn²⁺ additive. The emission decay times couldn't be measured due to short decay times which are according to literature in order of nanoseconds.



Graph 2. A comparison of emission intensities on shiny and dull side of pellets in dependence of Zn²⁺ additive concentration.

On graph 2, we can also observe that while maximum intensities of luminescence are growing uniformly when measured on shiny side of pellet, intensities of luminescence measured on dull side are erratic. This can be explained by pore sizes inhomogeneity in presintered pellets- the pellets have probably better pore size distribution on shiny side. This is also supported by the fact that the shiny side of pellet is concave after sintering due to better green body microstructure.

Due to necessity of high thermal etching temperature we used Band Contrast maps from EBSD measurements for determination of grain size distribution Fig. 1. The median grain size grows with growing sintering temperature

from 0.84μm (1300°C/2h) through 1.38μm(1400°C/2h) to 3.10μm(1500°C/2h).

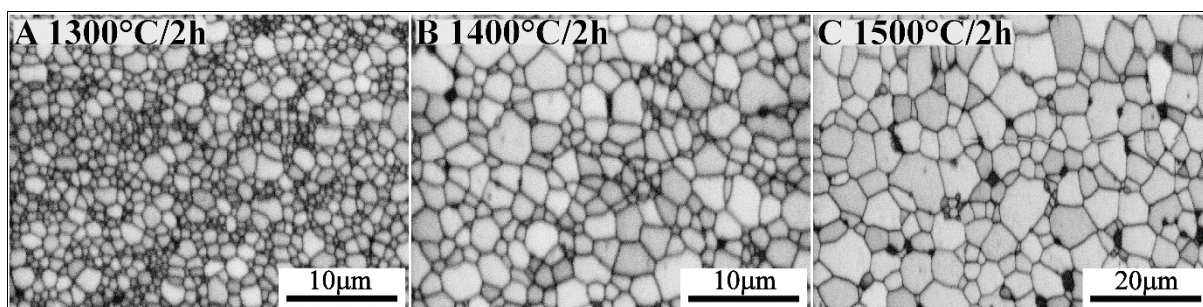


Fig. 1. Y₂O₃ : 3.5 at% Zn²⁺- Microstructure vs sintering temperature.

On Fig. 2 the SEM shows porous cross section of polished sample. Zinc oxide is concentrated into zincite grains detected by EBSD. EDXS confirms this and analysis shows mainly random signal(noise) of zinc where yttria grains are located. There are a few places where EDXS shows a zinc signal but no zincite is indexed by EBSD. This is probably caused by greater volume and measurement depth of EDXS. In some cases, the Y₂O₃ and ZnO Kikuchi patterns superposition during EBSD measurements made the phase indexing impossible.

The future work plans involve the measurements of sintered pellets densities using archimedes method and characterization of these specimens by XRD. If possible, the SEM of presintered sample will be done to determine pore distribution through pellet crosssection.

Keywords: Yttria ceramics, ZnO, Fluorescence, Pressure filtration

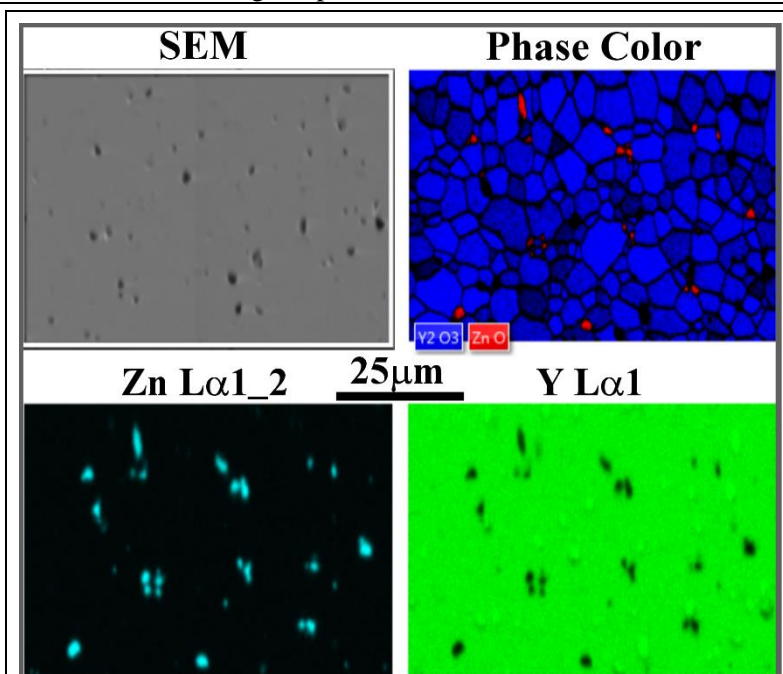


Fig. 2. SEM, EDXS and EBSD maps

Acknowledgment:



This paper is a part of dissemination activities of project [FunGlass](#).

This project has received funding from the European Union's Horizon 2020 research and innovation programme under grant agreement No 739566, SAS-MOST JRP 2015/6, VEGA 2/0026/17 and VEGA 1/0527/18.

From Xerogels to Aerogels: synthesis of porous oxyfluoride glass-ceramics for optical applications

J.J. Velázquez¹, J. Mosa², Y. Castro², D. Galusek³ and A. Durán²

¹Department of Coating Processes, FunGlass, Alexander Dubček University of Trenčín, Študentská 2, 911 50 Trenčín, Slovakia

(E-mail:jose.velazquez@tnuni.sk)

²GlaSS Group, Ceramic and Glass Institute (ICV-CSIC), 28049, Madrid, Spain

³Joint Glass Centre of the IIC SAS, TnUAD and FChFT STU, FunGlass, Študentská 2, 911 50 Trenčín, Slovakia

ABSTRACT

Rare-earth (RE) ions doped oxyfluoride glass-ceramics (OxGCs) are being widely investigated in the last decades for its potential use in different photonics applications, such as solid-state lasers, white light emitting diodes (wLEDs), solar cells and catalysis, among others. These materials combine the good mechanical, thermal and chemical properties of an oxide glass matrix with the low phonon energy of crystalline fluoride environments ($250\text{-}450\text{ cm}^{-1}$) and good solubility of RE ions in the fluoride crystals, which reduces non-radiative multiphonon relaxations, increasing the optical efficiency. Moreover, GCs present a high degree of transparency due to the much smaller size of uniformly dispersed nanocrystals (NCs) in the amorphous matrix, less than 100 nm [1,2]. These OxGCs can also be obtained in different forms, such as bulk, coatings or fibers.

One of the synthesis routes to obtain bulk OxGCs is the sol-gel method. The SG emerges as an alternative synthesis route at low temperatures, to avoid the drawbacks observed in other routes, such as the melting-quenching (MQ) process. This method permits obtaining more homogeneous and pure materials with higher fluorine content, resulting in high crystalline fraction, around 18 wt% in $80\text{SiO}_2\text{-}20\text{LaF}_3$ compositions [3,4]. However, bulk transparent SG materials are difficult to obtain due to the presence of the residual porosity in the structure and the existence of residual stresses generated during the sintering process [5]. Moreover, the presence of residual OH groups strongly reduces the RE ions luminescence.

To overcome these shortcomings the processing of bulk SG materials must be optimized. The first approximation combines the SG chemistry and the supercritical drying process to obtain $\text{SiO}_2\text{-REF}_3$ composite aerogels partially crystallized with a narrow pore size distribution. This process route is inspired by the drying procedure of silica aerogels under supercritical conditions, followed by adequate thermal treatments to obtain bulk OxGCs. Following this processing route, the synthesis was optimized to obtain bulk monolithic wet-gels, by controlling the synthesis and processing parameters (tetraethyl orthosilicate (TEOS)/water/ethanol ratio, pH, temperature and reaction time, rate of hydrolysis and condensation, aging time in ethanol, etc). Then, bulk materials were obtained using supercritical drying process under supercritical conditions of ethanol in CO_2 . However, despite the effective synthesis of monolithic crack-free samples, the performed DTA/DSC, FTIR, XRD analysis of the obtained bulk materials, after the different sintering process (temperature and time), revealed that the crystallization was strongly inhibited after the supercritical drying process using ethanol ($243\text{ }^\circ\text{C}$ and 72 Mpa).

Therefore, it was necessary to propose a new route to obtain bulk OxGCs, based on the use of transfer charge complexes to synthesize LaF_3 NCs. The NCs obtained this way can be incorporated into a TEOS/water/ethanol solution to obtain sols with $\text{SiO}_2\text{-REF}_3$ composition. These samples can be finally processed following different routes, such as supercritical drying or slow drying + thermal treatment resulting in crack-free bulk OxGCs [6,7]. Preliminary analysis of the materials obtained by this route reveals NCs with mean size ranging 5-8 nm obtained at very low temperature ($70\text{ }^\circ\text{C}$), opening the way to use in composite aerogels.

Keywords: Oxyfluoride glass ceramics; sol-gel; nanocrystal; supercritical drying; transfer charge complex process; optical properties.

References:

- [1] A. De Pablos-Martín,; A. Durán,; M.J. Pascual, *Int. Mater. Rev.* 57 (2012) 165.
- [2] P.P. Fedorov, A.A. Luginina, A.I. Popov, *J. Fluor. Chem.* 172 (2015) 22.
- [3] G. Gorni, J.J. Velázquez, J. Mosa, G.C. Mather, A. Serrano, M. Vila, G.R. Castro, D. Bravo, R. Balda, J. Fernández, A. Durán and Y. Castro, *Nanomaterials* 9 (2019) 530.
- [4] G. Gorni, J.J. Velázquez, J. Mosa, R. Balda, J. Fernández, A. Durán and Y. Castro, *Materials* 11 (2018) 212
- [5]. Kajihara K. *J Asian Cer Soc.* 1 (2013) 121.
- [6] F. Chaput, F. Lerouge, S. Tusseau-Nenez, P. Coulon, C. Dujardin, S. Denis-Quanquin, F. Mpambani, and S. Parola, *Langmuir* 27 (2011) 5555
- [7]. M. Odziomek, F. Chaput, F. Lerouge, C. Dujardin, M. Sitarz, S. Karpati, and S. Parola, *Chem. Mater.* 30 (2018) 5460.

Acknowledgment:



This paper is a part of the dissemination activities of project FunGlass. This project has received funding from the European Union's Horizon 2020 research and innovation programme under grant agreement No 739566.

Structural relaxation of PbO-WO₃-P₂O₅ glasses

M. Chromčíková^{1,2}, B. Hruška³, M. Liška^{1,2}

¹ VILA – Joined Glass Centre of the IIC SAS, TnUAD, FChPT STU, Študentská 2,
SK-911 50 Trenčín, Slovakia

(E-mail: maria.chromcikova@tuni.sk)

² VILA, FunGlass, A. Dubček University of Trenčín, Študentská 2, SK-911 50 Trenčín, Slovakia

³ Central Laboratories, FunGlass, Alexander Dubček University of Trenčín, Študentská 2,
SK-911 50 Trenčín, Slovakia

ABSTRACT

The structural relaxation of three compositional series of PbO-WO₃-P₂O₅ glasses with composition $(0.5 - x/2) \text{PbO} \cdot x\text{WO}_3 \cdot (0.5 - x/2) \text{P}_2\text{O}_5$, $x = 0, 0.1, 0.2, 0.3, 0.4, 0.5$; $0.5 \text{PbO} \cdot x\text{WO}_3 \cdot (0.5 - x) \text{P}_2\text{O}_5$, $x = 0, 0.1, 0.2, 0.3$; and $(0.5 - x) \text{PbO} \cdot x\text{WO}_3 \cdot 0.5 \text{P}_2\text{O}_5$, $x = 0, 0.1, 0.2, 0.3, 0.4, 0.5$ was studied by thermomechanical analysis [1, 2]. The relaxation was described using a mathematical model based on the stretched exponential relaxation function with relaxation time proportional to actual viscosity. The viscosity dependence on thermodynamic temperature and fictive temperature was expressed by Mazurin's approximation [3, 4, 5]. The relaxation parameters dependence on the glass composition was studied. It was found that the modulus is increasing with increasing amount of WO₃ in all glasses. On the contrary, the width of the spectrum of relaxation times is decreasing with increasing amount of WO₃ in all studied glasses.

Keywords: Phosphate glasses, Structural relaxation, Viscosity, Glass transition.

Acknowledgment:



This paper is a part of dissemination activities of project [FunGlass](#).

This project has received funding from the European Union's Horizon 2020 research and innovation programme under grant agreement No 739566.

This work was supported by The Slovak Grant Agency for Science under grant No. VEGA 2/0088/16, VEGA 1/0064/18.

References:

- [1] Koudelka L, Lissová M, Rosslerová I, Mošner P, Černošek Z, Liška M, Montagne L, Delevoye L, Delevoye L. Structure and properties of lead tungstate phosphate glasses. *Phys Chem Glasses: Eur J Glass Sci Technol B*. 2012;53:86–92.
- [2] Mošner P, Vosejpková K, Koudelka L, Montagne L, Revel B. Structure and properties of glasses in ZnO–P₂O₅–TeO₂ system. *J Non-Cryst Solids*. 2011;357:2648–52.
- [3] Mazurin OV. *Steklovanie Nauka*. Leningrad; 1986. p. 158.
- [4] Tool AQ. Relation between inelastic deformability and thermal expansion of glass in its annealing range. *J Am Ceram Soc*. 1946;29:240–53.
- [5] Liška M, Štubňa I, Antalík J, Perichta P. Structural relaxation with viscous flow followed by thermodilatometry. *Ceramics–Silikáty*. 1996;40:15–9.

Surface active components of glass forming melts identified by thermodynamic model

B. Hruška¹, M. Chromčíková^{2,3}, J. Micháľková⁴, Jana Vokelová-Vráblová⁴ and M. Liška^{2,3}

¹ Central Laboratories, FunGlass, Alexander Dubček University of Trenčín, Študentská 2, SK-911 50 Trenčín, Slovakia
(E-mail: branislav.hruska@tnuni.sk)

² VILA – Joined Glass Centre of the IIC SAS, TnUAD, FChPT STU, Študentská 2, SK-911 50 Trenčín, Slovakia

³ VILA, FunGlass, A. Dubček University of Trenčín, Študentská 2, SK-911 50 Trenčín, Slovakia

⁴ FunGlass, Alexander Dubček University of Trenčín, Študentská 2, SK-911 50 Trenčín, Slovakia

ABSTRACT

The use of thermodynamic models, especially the thermodynamic model Shakhmatkin and Vedishcheva (SVTDM) still has a wide application [1]. The glass composition proposed by us is derived from the needs of the glass industry. Using the FACT database [2] it is possible to find all the thermodynamic data needed to quantify the SVTDM.

In multi-component melts, there is a tendency to deistribute components so that the resulting surface energy is minimal. The substances that lower the surface tension concentrates in the surface layer of the melt. The surface tension enhancing components have a lower concentration in the surface layer than in the volume. E.g. oxides MgO, ZnO, BaO, ZrO₂, and Li₂O increase the surface tension of glass, however other oxides, especially K₂O, PbO a B₂O₃, decrease it [3].

A variety of methods are known for measuring the surface tension of liquid systems. The most reliable results can be obtained by analyzing the sessile and pendant drop profiles. The principle of the method lies in the regression analysis of the drop profile based on the numerical solution of the Laplace equation [4, 5].

The chemical composition of the studied glasses was designed as four compositional series. The glass batches were prepared from analytical grade purity oxides and carbonates. Glasses were melted in Pt crucible in superkanthal furnace at the temperature of 1600°C for two-three hours in ambient atmosphere. The chemical composition (Tab. 1) of studied glasses was analyzed by inductively coupled plasma optical emission spectroscopy (VARIAN - Vista MPX / ICP-OES). Sessile drops were prepared from the glass cubes of approximate (2×2×2) mm³ dimensions on glassy carbon plate (Fig. 1a) in the atmosphere of pure nitrogen. Pendant drops were obtained by melting of the T-shape glass samples suspended in the platinum wire ring (Fig. 1b). The drop profile was recorded by the CCD camera uEye (IDS Imaging Development Systems GmbH) and digitized using the Lucia[®] software (LIM, a.s., Prague).

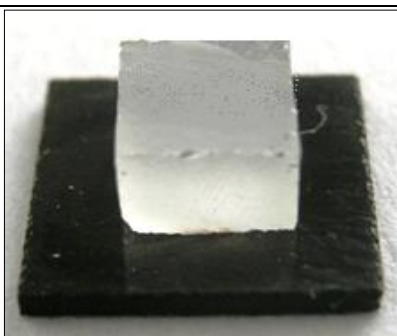


Figure 1: Sample prepared for the measurement by the sessile drop method.



Figure 2: Sample prepared for the measurement by the pendant drop method.

The surface tension was determined over the temperature range 1250-1500°C by the sessile and pendant drop methods. The values of surface tension were obtained by the least squares method by minimization of the sum of squares of deviations between the experimental and calculated drop profile. The calculated drop profile was obtained by the numerical integration of the Laplace equation using the experimental

density values.

The ZnO component was identified as the surfactant based on the significant negative correlation of its amount with the surface tension value. The surface tension values obtained by the sessile drop method were in almost all cases little bit lower than those obtained by the pendant drop method. On the other hand the values are identical within the estimated standard deviation.

Table 1: *Glass composition in mole percent of oxides as analyzed.*

Glass	Na ₂ O	K ₂ O	CaO	ZnO	ZrO ₂	SiO ₂
NKCZ1	7.64	7.36	8.61	-	0.95	75.44
NKCZ3	7.54	7.44	8.84	-	2.86	73.32
NKCZ5	7.74	6.89	9.97	-	5.12	70.28
NKCZ7	7.66	7.01	9.98	-	7.18	68.17
NKzZ1	7.45	7.41	-	10.08	0.98	74.08
NKzZ3	7.30	7.06	-	9.63	2.61	73.40
NKzZ5	7.66	7.13	-	10.92	5.22	69.07
NKzZ7	7.83	7.00	-	11.03	7.54	66.6
NCzZ1	13.51	-	4.80	4.58	0.89	76.22
NCzZ3	13.72	-	4.72	5.01	2.71	73.84
NCzZ5	15.78	-	5.13	5.58	5.42	68.09
NCzZ7	15.78	-	5.11	5.43	7.4	66.29
KCzZ1	-	15.81	5.03	5.27	1.01	72.88
KCzZ3	-	13.95	4.47	4.95	2.66	73.97
KCzZ5	-	13.64	4.97	5.48	5.20	70.72
KCzZ7	-	13.88	4.98	5.43	7.25	68.46

Keywords: Thermodynamic model, Shakhmatkin and Vedishcheva, surface tension

Acknowledgment:



This paper is a part of dissemination activities of project [FunGlass](#). This project has received funding from the European Union's Horizon 2020 research and innovation programme under grant agreement No 739566 and in the frame of the project Centre for Functional and Surface Functionalized Glass (CEGLASS), ITMS code is 313011R453, operational program Research and innovation, co-funded from European Regional Development Fund

This work was supported by The Slovak Grant Agency for Science under grant No. VEGA 2/0088/16, VEGA 1/0064/18.

References:

- [1] J. Macháček, M. Chromčíková, M. Liška: Parameterization and Validation of Thermochemical Models of Glass by Advanced Statistical Analysis of Spectral Data. In *Thermal Physics and Thermal Analysis: From Macro to Micro, Highlighting Thermodynamics Kinetics and Nanomaterials*. J. Šesták, P. Hubík and J. J. Mareš (Editors), Chapter 12, p. 257-278, Springer, Switzerland 2017. ISBN 978-3-319-45897-7.
- [2] C.W. Bale, P. Chartrand, S.A. Deckerov, G. Eriksson, K. Hack, R. Ben Mahfoud, J. Melancon, A.D. Pelton and S. Petersen: *Calphad*, 62, 189-228 (2002); www.crct.polymtl.ca/fact/.
- [3] J. Hlaváč: *Základy technologie silikátů*. 2. vyd. Praha : SNTL, 1988, 516 s.
- [4] A. Kalantarian, S. M. I. Saad, A.W. Neumann: Accuracy of surface tension measurement from drop shapes: The role of image analysis. *Advances in Colloid and Interface Science* 199–200 (2013) 15–22.
- [5] J. D. Berry, M. J. Neeson, R. R. Dagastine, D. Y. C. Chan, R. F. Tabor: Measurement of surface and interfacial tension using pendant drop tensiometry. *Journal of Colloid and Interface Science* 454 (2015) 226–237.

HP sintering of yttrium-aluminate glass-Impact of particle size distribution on mechanical properties

^{1,2}Anna Prnová, ^{1,2}Jana Valuchová, ³Žaneta Dohnalová, ⁴Ondrej Hanzel, ²Robert Klement, ⁵Els Bruneel, ^{1,2}Dušan Galusek

¹Join Glass Centre of the IIC SAS, TnUAD, FChPT STU, Študentská 2, 911 50 Trenčín, Slovakia

²FunGlass, A. Dubček University of Trenčín, Študentská 2, 911 50 Trenčín, Slovakia

³Institute of Inorganic Chemistry, Slovak Academy of Sciences, Dúbravská cesta 9, 845 36 Bratislava, Slovak Republic

⁴Department of Inorganic Technology, Faculty of Chemical Technology, University of Pardubice, Doubravice 41, 532 10 Pardubice, Czech Republic

⁵Department of Inorganic and Physical Chemistry, Gent University, Krijgslaan 281 (53), 9000 Gent, Belgium

Email: anna.prnova@tnuni.sk

ABSTRACT

The samples AYEM, AYEMB and AYEMFD, containing 76.8 mol.% Al_2O_3 and 23.2 mol.% Y_2O_3 were prepared by three different ways. The combination of modified Pechini sol-gel method and flame synthesis was used for preparation of AYEM sample. The prepared glass microspheres (AYEM) were subsequently ground in vibratory mill (Fritsch Pulverisette 0) for 30, 45, 60, 75, 90, 105, 120, 150, 180, 210 and 240 min with amplitude 1.0 mm and marked as samples AYEBM1-AYEBM11. For preparation of AYEMFD sample, the combination of sol-gel Pechini method, freeze-drying and flame synthesis was used. All prepared systems were studied by using of XRD, DTA, PSA and SEM analysis. Preliminary HP and RHP experiments were performed. The Vickers hardness 16.6 – 17.0 GPa was obtained in sintered samples. The morphology of prepared glass-ceramics materials were examined by scanning electron microscopy and the results are reported.

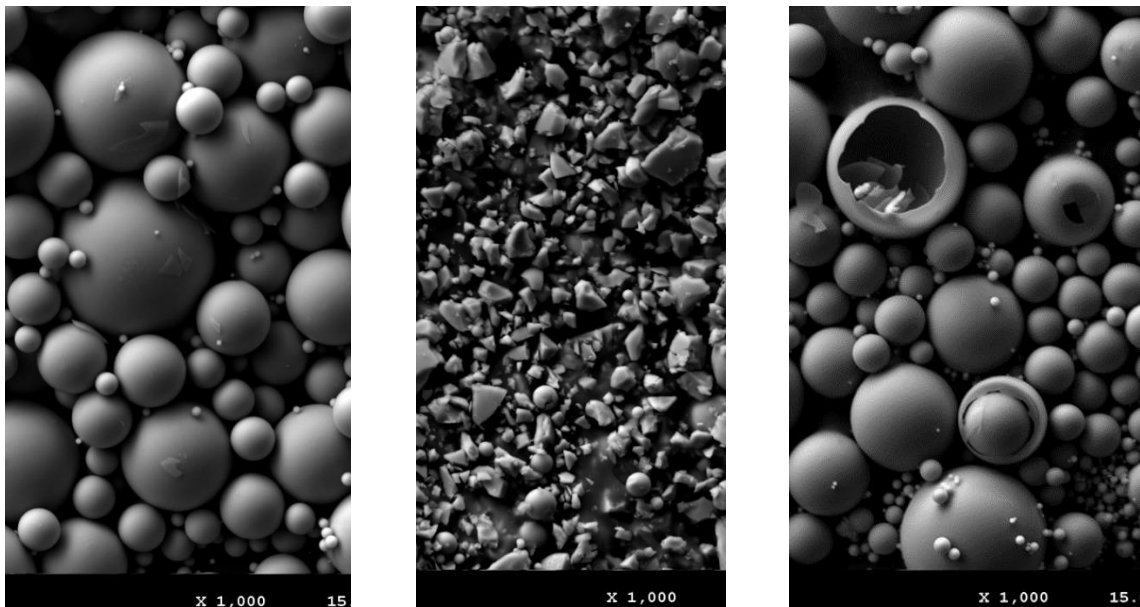


Fig.1. SEM images of AYEM sample (a), grinding sample AYEBM11 (b) and freeze-dried sample AYEMFD (c).

Funding Statement



This paper is a part of dissemination activities of project FunGlass. This project has received funding from the European Union's Horizon 2020, research and innovation programme under grant agreement No 739566. The financial support of this work by the projects APVV 0014-15, APVV 0049-17, VEGA 1/0527/18, VEGA 2/0026/17, VEGA 2/0088/16, VEGA 1/0064/18 is gratefully acknowledged.

Preparation of YAG glass from glass microspheres

M. Micháľková¹, J. Kraxner² and D. Galusek³

¹ Vitrum Laugaricio – Joint Glass Center of the IIC SAS, TnU AD, and FChPT STU, Trenčín, Slovakia,
(E-mail: monika.michalkova@tnuni.sk)

² Glass processing department, FunGlass – Centre for Functional and Surface Functionalized Glass

³ Director of FunGlass – Centre for Functional and Surface Functionalized Glass

ABSTRACT

A glass, whether in bulk, fibre, or film form, is a non-crystalline solid (NCS) which undergoes a glass transition, to which is associated a glass transition temperature, T_g . In principle, any substance can be vitrified by quenching it from the liquid state, while preventing crystallization, into a solid glass, with the melt structure becoming “frozen” below T_g [1].

In this work, we present our recent research on preparation of bulk YAG glass from YAG glass microspheres. Sol-gel process's (Pechini method) prepared YAG powder was fed into a high temperature methane-oxygen flame (estimated temperature 2800 °C), where the particles melted and YAG glass microspheres were formed. Molten droplets were quenched at the estimated cooling rate 1000 °C/min by spraying them with deionized water to prevent crystallization, and the formed glass microspheres were collected. Viscous flow sintering of YAG glass microspheres were then used to prepare bulk YAG glass in hot press. This is a well-known method in which free surfaces are eliminated by viscous flow at temperatures above T_g . However, many quenched glasses crystallize rapidly at temperatures T_x when the supplied thermal energy mobilizes the structure and the latent heat previously trapped during quenching is released [2]. Crystallization can therefore be observed even during hot-pressing (Fig. 1) by changing of the heating rate slope (measured by thermocouple placed beneath the sample). When crystallization occurs dilatation of the sample stops within few seconds. Which means the amount of residual glass in the sample is so low that elimination of free surfaces by viscous flow is not possible anymore.

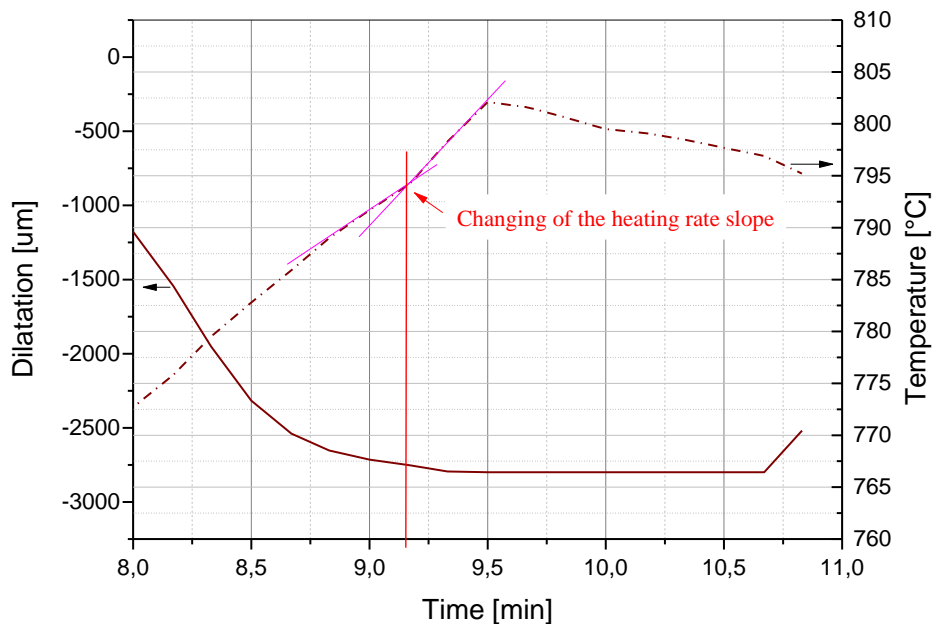


Figure 1: Dilatation of YAG sample during hot-pressing as a function of time and changing of sample's temperature vs time.

The working temperature of such glasses is thus restricted to be between T_g and T_x so called kinetic

window [2]. According to DSC measurements (Fig. 2) between T_g inflection and T_x onset is 24 °C at the heating rate 5 °C/min. Additionally, during experiment we have to take into account the heat capacity of the carbon die. Therefore, experiments were planned according to dilatation data from hot-press (Fig. 2.)

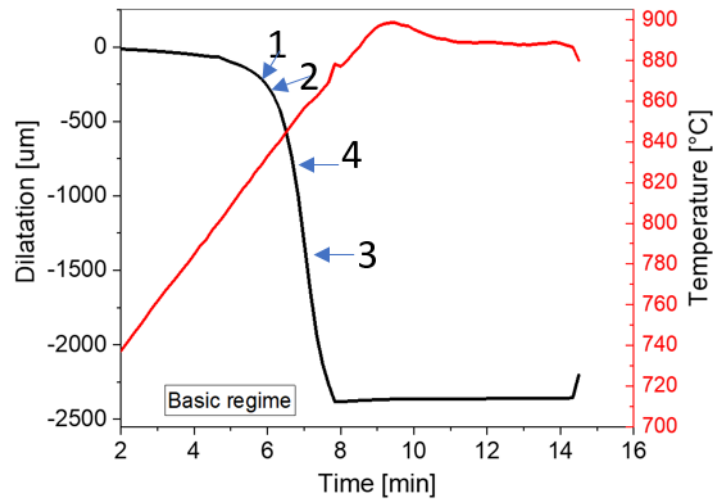


Fig. 2.: Dilatation of YAG sample during hot-pressing as a function of time and changing of sample's temperature vs time.

Careful optimisation of the sintering conditions lead to the YAG bulk glass/ceramic with the relative density over 99 % with 6 wt. % of crystalline phase.

Keywords: DSC, XRD, YAG.

Acknowledgment:



This paper is a part of dissemination activities of project [FunGlass](#). This project has received funding from the European Union's Horizon 2020 research and innovation programme under grant agreement No 739566.

References:

- [1] M. Almeida and M. Clara Goncalves: Crystallization of Solgel-Derived Glasses. *International Journal of Applied Glass Science*, 5 [2] 114–125 (2014).
- [2] A. Rosenflanz et al.: Bulk glasses and ultrahard nanoceramics based on alumina and rare-earth oxides. *Nature*, 430, 761-764 (2004).

Vitrification and upcycling of inorganic waste

Miroslava Hujova¹, Jozef Kraxner¹

¹ Department of Glass Processing, FunGlass, Alexander Dubček University of Trenčín,
Trenčín, Slovakia
(E-mail: miroslava.hujova@tnuni.sk)

ABSTRACT

The vitrification of wastes is in general accepted as a reliable way to stabilize dangerous and hazardous wastes in the form of glass. One of the world's most complex vitrification projects, the Hanford Waste treatment and immobilization plant (USA) [1], was launched as a response to, what was up until very recently, the most severe nuclear pollution in the Western hemisphere. This clean-up project has gathered tremendous amounts of data on how to turn the radioactive and toxic nuclear waste into a stable glass. This waste is in the form of slurries, which contain over 60 elements, and are stored in 177 underground tanks. Each tank needs to be treated separately, the suitable glass forming and modifying additives need to be tailored to their unique composition and only then can the slurry be vitrified. After long years of research, the Hanford area clean-up will be finally launched in 2022 [2].

This particular issue of nuclear pollution could be perceived as non-relatable in Europe, where in general the vitrification of nuclear fission byproducts is the subject of well-working technology. However, with growing consumer demand, and the ever growing industrial production, the issue of environmental pollution is becoming a grievous global issue of the 21st century [3]–[7]. The recycling of used materials is no longer sufficient, and in recent years it has also failed in many areas. The most significant area is the failure to process chemical variations of the same material (i.e. plastics), or to even address potential recycling of composite materials. The best example would be solar collectors, where vast numbers of them will be obsolete in the next few decades. That will add just another item to the ever-growing list of inorganic and partially inorganic waste streams, which already include waste from the glass making industry (glass shards, cutting debris, insulations), mining sites (byproducts from ore), ashes from incineration sites, TV screens, medical waste etc. [3].

Another setback of recycling is that it demands proper separation of the waste for the desired recycling stream, and leaves behind a significant share of final waste that ends in landfills, which are rapidly growing in price [8]. This is one of the main reasons why governments and industry are very reluctant to invest more into this technology, which only gets a marginally positive net balance against the full-landfill solution.

Hanford's ability to turn waste streams into stable glass could be the inspiration for the launch of inorganic vitrification projects in Europe and worldwide. The vitrification could provide a solution to toxic, stable and obsolete materials, which do not have alternative solutions nowadays. However, if the aim of the vitrification would only be the reduction of waste volume via the waste glass designated for landfill, due to expenses, there would only be a little motivation on the market economy to actually participate [9].

Therefore, the aim for the inorganic waste vitrification should not be the production of waste glasses, but of the products that would re-enter market as novel and attractive materials. For example, if a consolidated vitrification product enters flame synthesis, it could result in the formation of glasses with novel composition and applications. One such application could be in the popular, and growing, 3D printing technology (AMT-Additive Manufacturing Technology). Another possibility is the design and manufacturing of building materials from insulations to construction parts that would bring longer durability, better mechanical properties or would replace decoration materials, i.e. marble, which nowadays comes at the cost of the destruction of natural sites [4].

However, in the first step, there needs to be a cooperation with industry partners from the mid-European area, and also with the research institutions in that area. A library of partner sites is

currently built with information on waste type and volume and then from the obtained samples, the general composition for particular waste streams (i.e. via XRF, SEM-EDS/WDS, XRD) will be added as well. In the second step, after the example of the Hanford project, target glasses would be designed for a particular purpose and could also open the door to the idea of recycling-upcycling in the research of novel materials and composites for targeted applications with better chemical, physical and mechanical properties than existing materials.

Keywords: Recycling, Upcycling, Waste management, Vitrification, Flame synthesis, AMT, Foam glass.

Acknowledgment:



This paper is a part of dissemination activities of project [FunGlass](#).
This project has received funding from the European Union's Horizon 2020 research and innovation program under grant agreement No 739566.

References:

- [1] K. S. Matlack *et al.*, "DM100 and DM1200 Melter Testing with High Waste Loading Glass Formulations for Hanford High-Aluminum HLW Streams, VSL-10R1690-1," Vitreous State Laboratory, The Catholic University of America, Washington, DC, 2010.
- [2] J. D. Vienna, "Nuclear Waste Vitrification in the United States: Recent Developments and Future Options," *Int. J. Appl. Glas. Sci.*, vol. 1, no. 3, pp. 309–321, Sep. 2010.
- [3] P. Colombo, G. Brusatin, E. Bernardo, and G. Scarinci, "Inertization and reuse of waste materials by vitrification and fabrication of glass-based products," *Curr. Opin. Solid State Mater. Sci.*, vol. 7, no. 3, pp. 225–239, 2003.
- [4] A. Rincón, M. Marangoni, S. Cetin, and E. Bernardo, "Recycling of inorganic waste in monolithic and cellular glass-based materials for structural and functional applications," *J. Chem. Technol. Biotechnol.*, vol. 91, no. 7, pp. 1946–1961, 2016.
- [5] P. C. Enrico Bernardo, Giovanni Scarinci, "Vitrification of Waste and Reuse of Waste-Derived Glass," in *Encyclopedia of Sustainability Science and Technology*, 2017, pp. 1–34.
- [6] A. Rincon Romero, M. Salvo, and E. Bernardo, "Up-cycling of vitrified bottom ash from MSWI into glass-ceramic foams by means of 'inorganic gel casting' and sinter-crystallization," *Constr. Build. Mater.*, vol. 192, pp. 133–140, 2018.
- [7] E. Bernardo, L. Esposito, E. Rambaldi, A. Tucci, Y. Pontikes, and G. N. Angelopoulos, "Sintered esseneite-wollastonite-plagioclase glass-ceramics from vitrified waste," *J. Eur. Ceram. Soc.*, vol. 29, no. 14, pp. 2921–2927, 2009.
- [8] J. C. Marra and C. M. Jantzen, *Glass - An environmental protector*, vol. 83. 2004.
- [9] G. Meylan, R. Seidl, and A. Spörri, *Transitions of municipal solid waste management. Part I: Scenarios of Swiss waste glass-packaging disposal*, vol. 74. 2013

Dielectric properties of Barium Crystal Galss

Katarína Faturíková¹, Marek Liška^{2,3}, Peter Viščor⁴

¹ Central Laboratories, FunGlass, Alexander Dubček University of Trenčín, Študentská 2, SK-911 50 Trenčín, Slovakia

² VILA – Joined Glass Centre of the IIC SAS, TnUAD, FChPT STU, Študentská 2, SK-911 50 Trenčín, Slovakia

³ VILA, FunGlass, A. Dubcek University of Trenčín, Študentská 2, SK-911 50 Trenčín, Slovakia

⁴ EIS Laboratory, Skjoldenaesvej 17, 4174 Jystrup, Denmark

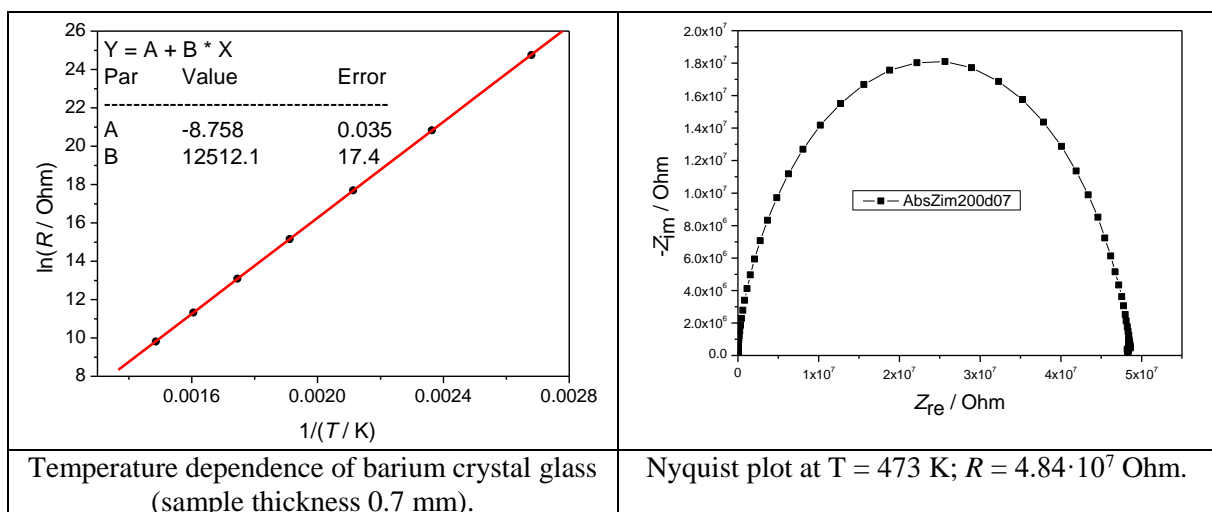
ABSTRACT

Complex impedance spectroscopy is flexible tool for simultaneous electrical and dielectrical characterization of materials. This powerful technique has been widely used to characterize the dielectric behaviour of single crystal, polycrystalline and amorphous materials [1-4].

In a typical EIS experiment, the complex electrical impedance of a sample is measured as a function of frequency over a wide frequency range – typically several orders of magnitude. From an experimental point of view, performing impedance analysis at frequencies below some MHz is a straightforward procedure, but the physical interpretation of experimental data is quite often rather complex. A frequently used method to analyze impedance data is modelling of the impedance spectra by an appropriate equivalent circuit. Graphically the experimental data are often plotted as the so-called Nyquist diagram, i.e. a plot of the negative imaginary part of the impedance $-Z''$ versus its real part Z' [5]. When measurements are carried out at different temperatures, it is possible to determine the activation energies of the conduction and dielectric relaxation processes.

The temperature dependence of the impedance spectra of the barium crystal glass was studied at temperatures (50, 100, 150, 200, 250, 300, 350, and 400)°C, in the frequency range from 1mHz to 1 MHz. Samples with thickness 0.7mm, 1mm, 1.7mm and 2.5mm were studied and compared. The temperature dependence of the DC resistance, R , estimated from the Nyquist plots has been analyzed. At higher temperature, the conductivity versus inverse thermodynamic temperature is exponential and can be explained by a thermally activated transport of Arrhenius type:

$$\ln(R/\text{Ohm}) = \ln k_{\text{resist}} + \frac{E_{\text{resist}}^{\ddagger}}{R_{\text{gas}} T}$$



Keywords: electrical impedance spectroscopy, dielectric properties, barium glass

Acknowledgment:



This paper is a part of dissemination activities of project [FunGlass](#).
This project has received funding from the European Union's Horizon 2020
research and innovation programme under grant agreement No 739566.

References:

- [1] BARSOUKOV E., MACDONALD J.R.: Impedance spectroscopy: Theory, Experiment and Applications, New Jersey: Wiley, 2005. ISBN 0-471-64749-7.
- [2] JAMES A.R., PRIYA S., UCHINO K., SRINIVAS K.: J. Appl. Phys., 90 (7), 3504, 2001.
- [3] LANFREDI S., CRAVLHO J.F., HEMANDES A.C.: J. Appl. Phys., 88 (1), 283, 2000.
- [4] SAAD ESMAT ABDEL-FATTAH I. . Dielectric properties of molybdenum oxide thin films. Journal of optoelectronics and Advanced Materials Vol. 7, No. 5, October 2005, p. 2743 – 2752.
- [5] SHARMA M.V.N.V.D., SARMA A.V., RAO R. BALAJI. Electrical characterization and relaxation behaviour of lithium-indium-phosphate glasses via impedance spectroscopy. Turk J. Phys., 2009; 33, 87-100.

Chemical Durability of Glass Fibres Insulation used in Nuclear Power Plants

J. Micháľková^{*1}, J. Vokelová¹, B. Hruska², M. Chromčíková^{3,4}, M. Liška^{3,4}

¹ FunGlass, Alexander Dubček University of Trenčín, Študentská 2,
SK-911 50 Trenčín, Slovakia
(E-mail: jaroslava.michalkova@tnuni.sk)

² Central Laboratories, FunGlass, Alexander Dubček University of Trenčín, Študentská 2,
911 50 Trenčín, Slovakia

³ VILA – Joined Glass Centre of the IIC SAS, TnUAD, FChPT STU, Študentská 2,
SK-911 50 Trenčín, Slovakia

⁴ VILA, FunGlass, A. Dubcek University of Trenčín, Študentská 2,
SK-911 50 Trenčín, Slovakia

ABSTRACT

In the case of the loss of coolant accident (LOCA) the glass fibres used as thermal and electrical insulation in PWR type nuclear power plant get in immediate contact with cooling solution of the emergency cooling system. Corrosion products formed during the contact insulation fibres with aggressive cooling solution can cause changes, resulting in insufficient even functionless operation of the cooling system. To assure safety of the cooling system it is important to know and describe behavior of insulating fibres in aggressive environment. Therefore the present work concerns chemical durability of the NUKON glass fibres used as insulating materials in nuclear power plants. Describes the static and dynamic tests, kinetics of transfer of the glass into the solution Tests were conducted in two corrosive medias - distilled water and corrosion solution $H_3BO_3/Na_2B_4O_7$ at temperatures 70 °C, 80 °C and 90 °C. Content of the elements was determined by atomic emission spectrometry with inductively coupled plasma VARIAN - Vista MPX/ICP-OES. Changes on the surface of the tested samples were observed by using scanning electron microscopy with energio-dispersion spectroscopy. Time dependences of normalized quantities of individual elements were described by regression function designed by Helebrant's model. From the results of static and dynamic tests follows that normalized elements in distilled water at different temperatures have different course than in the corrosive solution $H_3BO_3/Na_2B_4O_7$ and with increasing temperature tends to increase the normalized quantity of leaching elements in various corrosive solutions. The values of normalized quantities of elements set out in both corrosive solutions provided comparable results with values translated by empirical equation.

Keywords: Glass fibres, thermal insulation, LOCA, coolant solution, chemical durability, corrosion.

Acknowledgment:



This paper is a part of dissemination activities of project [FunGlass](#).
This project has received funding from the European Union's Horizon 2020 research and innovation programme under grant agreement No 739566.
This work was supported by The Slovak Grant Agency for Science under grant No. VEGA 2/0088/16, VEGA 1/0064/18 and APVV 0487-11.

References:

- /1/. MAHMOODI, R., SHARIARI, M., ZOLFAGHARI, A., MINUCHEHR A.: *An advanced method for determination of loss of coolant accident in nuclear power plants*, Nuclear Engineering and Design 241, 2013–2019, (2011)
- /2/. OBDRLÍKOVÁ, V.: *Koroze izolačních vláken pro jaderné elektrárny*. Diplomová práce, VŠCHT Praha, (2013).
- /3/. CHROMČÍKOVÁ, M. – VOKELOVÁ, J. - MICHÁLKOVÁ, J. - LIŠKA, M. - MACHÁČEK, J. GEDEON, O. - SOLTÉSZ, V.: *Chemical durability of gamma-irradiated glass fibrous insulation*. J. Nuclear Technology 193, 297-305, (2016).

Characterization of Ce-doped yttria ceramics prepared by pressure filtration

Nibu Putenpurayil Govindan¹, Monika Micháľková², Dušan Galusek¹,

¹ – FunGlass - Centre for functional and surface functionalized glass, TnUAD, Trenčín, Slovakia
(E-mail:nibu.puthenpurayil@tnuni.sk)

² - Vitrum Laugaricio – Joint Glass Center of the IIC SAS, TnU AD, and FChPT STU, Trenčín, Slovakia,

Cerium doped yttrium oxide ($Y_2O_3:Ce^{3+}$) nanopowders have been synthesized using precipitation method (1-3) with ammonium hydroxide used as a precipitation agent. The aqueous nitrate solution of Y^{3+} was prepared by dissolving yttria powder (99.99 %) in diluted nitric acid (HNO_3) under continuous stirring at $90^\circ C$ and then diluted into 0.1 M with deionized water. The 0.1M solution of Ce^{3+} was prepared by dissolving cerium nitrate (99.99 %) in deionized water. The mixed metal nitrate solution was dripped into ammonium solution, under continuous rapid stirring, ensuring there was sufficiently high excess of ammonia to eliminate any pH fluctuations throughout the process. The mixed solution turned to opaque white slurry. After 12 h aging the slurry was vacuum filtered through filter paper and the resulting white precipitate was washed with distilled water, dried overnight in air at $100^\circ C$, crushed and ground with pestle in an agate mortar, and calcined in air for 3 h at $700^\circ C$ (heating rate $10^\circ C/min$). Partly agglomerated powders with the primary size of Y_2O_3 nanoparticles ~ 55 nm and cubic crystal structure were prepared. The precipitation method led to severe agglomeration of ceria doped yttria powder. The powder had to be subjected to efficient de-agglomeration before it could be used for preparation of green compacts. The green compacts were prepared by vacuum-pressure filtration of prepared alcoholic suspension and reached relative density above 43 %.

Figure 1 shows the SEM micrograph of synthesized Ce^{3+} -doped Y_2O_3 powders. The powder is agglomerated with the primary particle size of approximately 55 nm, which is in good accord with the X-ray diffraction data. All ceria doped samples show the same particle size and all samples are agglomerated. Doping of yttria powder by ceria did not have any significant effect on particle size and distribution.

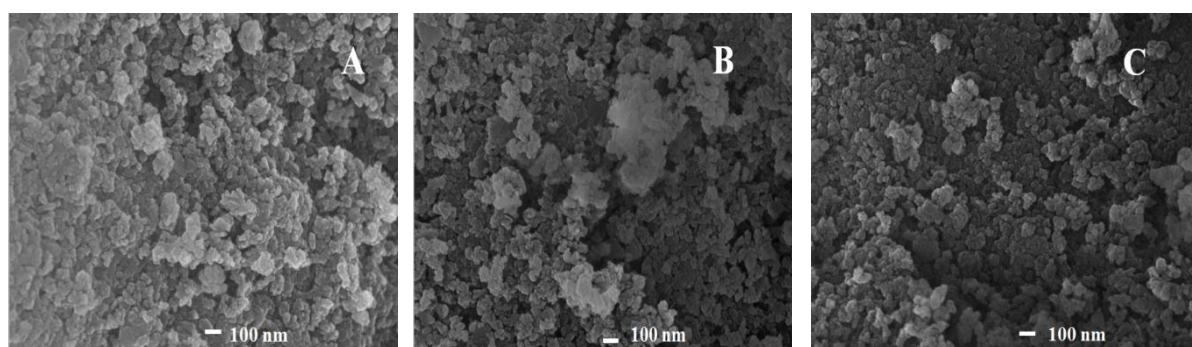


Fig 1: SEM micrograph of the synthesised Ce^{3+} -doped Y_2O_3 powder, A) 0.001 mol% Ce, B) 0.005 mol % Ce, C) 0.01 mol % Ce

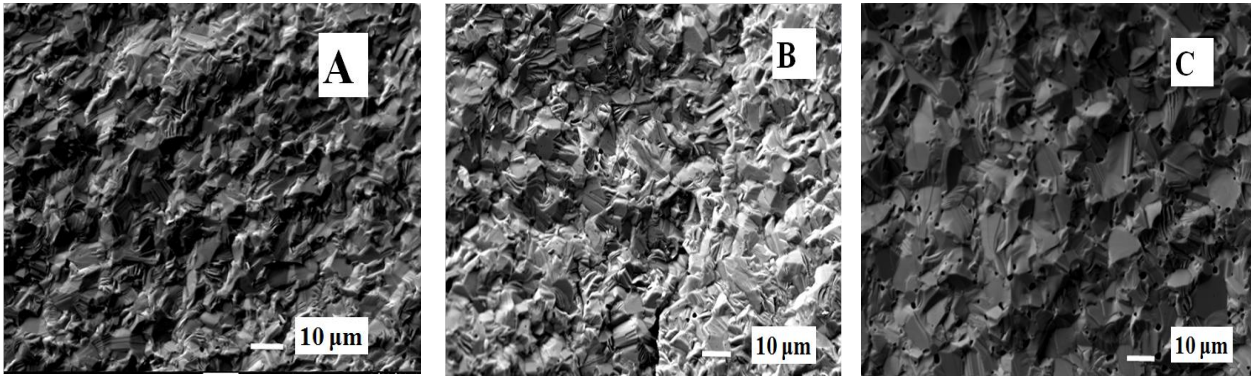


Fig. 2 Fracture surfaces of Y_2O_3 sintered ceramics prepared from Ce^{3+} doped powders, A) 0.001 mol % Ce, B) 0.005 mol % Ce, C) 0.01 mol % Ce

Figure. 2 shows the fracture surfaces of sintered Ce^{3+} doped yttria ceramics. SEM analysis of all ceria doped materials displayed microstructure with closed porosity, which could be used as starting material for hot isostatic pressing. **Table 1** summarizes the relative densities of all Ce^{3+} doped yttria samples after sintering at 1550 °C.

Table 1: Relative density of Ce^{3+} doped yttria ceramic prepared by pressure filtration method, sintered at 1550°C for 3h.

Ce^{3+} doped yttria	Relative density
0.001 Ce^{3+}	97.88 %
0.005 Ce^{3+}	98.38 %
0.01 Ce^{3+}	98.57 %

ACKNOWLEDGMENT



This paper is a part of dissemination activities of the project FunGlass. This project has received funding from the European Union's Horizon 2020 research and innovation programme under grant agreement No 739566. Financial support of this work by the grants VEGA 2/0026/17, and SAS-MOST 2015-06 is gratefully acknowledged.

REFERENCES

- [1] D. Sordélet, *Journal of Colloid and Interface Science*, 122, 47-59, (1988).
- [2] M. Ciftcioglu, *Journal of American Ceramic Society*, 70, 329-334 (1987)
- [3] T. Chartier T. *Journal de Physique Archives* 5.689-695. (1990)